Influence of concentration, type and particle size of fillers on the dynamic mechanical behaviour of elastomeric HTPB binder

Manfred A. Bohn [1], Mauricio Ferrapontoff Lemos [2, 1], Günter Mussbach [3, 1]

[1] Fraunhofer Institut für Chemische Technologie (ICT), Pfinztal, Germany
[2] Brazilian Navy Research Institute, Rio de Janeiro, RJ, 21931-090, Brazil
[3] Bayern-Chemie GmbH, D-84544 Aschau am Inn, Germany

Abstract

Recently, it was found that the second peak of the loss factor curve determined by DMA of HTPB bonded composite propellants and high explosives can change significantly in intensity and shape with composition. Composite propellants with AP, whereby the AP particles are connected via bonding agents to the binder matrix, can show a pronounced second peak, whereas HMX and RDX produce a weaker peak and with high contents of them, it can show only as shoulder attached to the first peak. The second peak is much more sensitive to ageing and to de-wetting. This means interactions between filler and matrix influence the appearance of the peak. Therefore, a more detailed investigation was started to elucidate the influences of fillers on the loss factor curve. Polyurethane binders made from polyol HTPB and isocyanate IPDI were filled with 20, 40 and 60 mass-% of ammonium perchlorate (AP), aluminum (Al) or RDX, using fine and coarse particles. For obtaining the cured composite, a special turning device constructed and manufactured at Fraunhofer ICT was installed inside the curing oven in order to avoid sedimentation of the fillers during curing. The composites were characterized by DMA in torsion mode from -100°C to +70°C, and the quality of distribution of fillers was evaluated by X-ray micro-tomography, which showed homogenous distribution of the filler particles in the samples. The part of loss factor tanδ at lower temperatures originates from the glass-rubber transition of the binder parts, which are unrestricted in mobility. This is defined in this way in comparison of the second broader peak at the high temperature side of the first peak, which is caused by binder parts restricted in mobility. The temperatures at each maximum are called Tg^{unr} and Tg^{res}, respectively. The results are: AP and RDX cause more changes in intensity of the first main peak in tanδ than Al particles. The maximum temperature Tg^{unr} is nearly not changed by any of the fillers. The changes in tanδ intensity determined from baseline corrected loss factor curves and modelled by EMG (exponentially modified Gauss) distributions indicate that Al has a stronger interaction with HTPB binder than AP and RDX particles. The particle sizes of AP and RDX and probably their shapes effect the viscoelastic properties. Increasing content of AP and RDX increase the storage shear modulus G' and somewhat the loss shear modulus G'', but as a whole tanδ intensity is lowered in the main peak.

Keywords: AP; aluminum; RDX; HTPB; filler effects on loss factor; DMA loss factor modelling

1. Introduction

In a series of investigations [1 to 14] it was found that the second peak in the DMA loss factor curve of HTPB (hydroxyl terminated polybutadiene) bonded composite rocket propellants (CRP) can change significantly with composition. AP (ammonium perchlorate) bonded with bonding agents to the binder matrix causes a pronounced peak see Fig. 1, curve CRP1, whereas HMX and RDX show only a small peak, see Fig.1 curve HX1, which changes to a shoulder with high degree of filling, see Fig. 1, curve HX2. Up to now for HMX and RDX no such bonding agents exist as for AP. Total intensity and position of the maxima is also deter-

Paper number 20069, Text pages 1 to 30, Session 3B, on 2018 NDIA-IMEMTS, event number 8550, April 23-29, 2018, Portland Oregon, USA. http://www.ndia.org/events/2018/4/23/imem

mined by the used plasticizer and its amount and somewhat by the curing agent [2, 5, 15 to 18]. The second peak is also very ageing dependent [1,4,7,12 to 14], especially with HTPB-based binders. In spite of the presence of antioxidants, ageing happens, when oxygen access is possible. Surely, the ageing rate is reduced by antioxidants, but it is not brought to zero. The ageing causes additional cross-links between binder chains and reduces the strain capacity of the formulation. This second peak is also indicative for de-wetting between binder and filler particles. From all observations it becomes evident that intermolecular interactions between filler and binder matrix are important [20, 21].

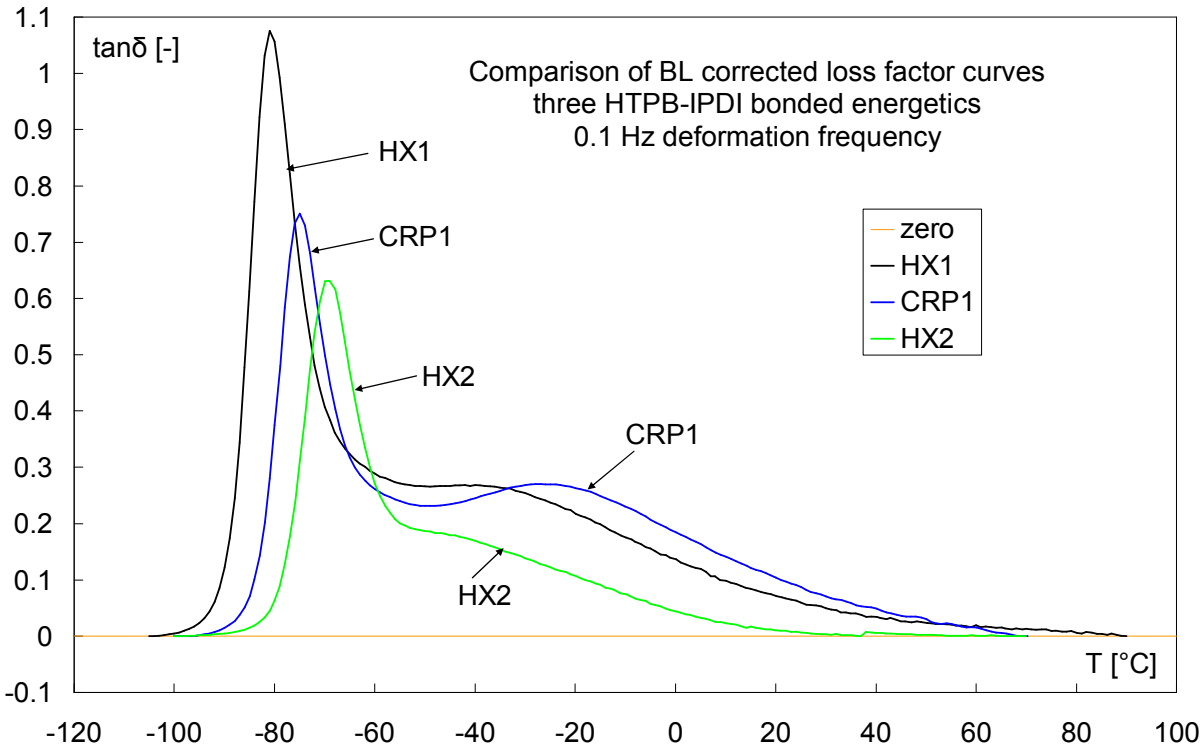

Figure 1: Three examples of loss factor, all obtained by torsion DMA and with substances based on HTPB-IPDI binder. The principle structure is equal with all three formulations. The main components in mass-% are, besides antioxidant (AO) and bonding agent (BO):

CRP1	HTPB-IPDI (12),	AP (78), Al (6),	DOA (4, 25% of binder), AO, BO
HX1	HTPB-IPDI (12),	RDX (80),	DOA (8, 40% of binder), AO
HX2	HTPB-IPDI (14),	HMX (85),	DOA (1, 6,7% of binder), AO

The aim is therefore to perform detailled experimental investigations on the influences of the typical fillers AP, Al (aluminium) and RDX on the loss factor intensity and loss factor shape and on its shift in temperature with deformation frequency. It is intended to find out, in which way the different filler types interact with the binder. In a first step of investigation, three filler types are selected and formulations with three different contents, 20, 40 and 60 mass-% are manufactured, including coarse and fine particles.

2. Experimental

2.1 Substances

The binder comprises of HTPB R45 HTLO (from Sartomer, Polybd, Oakland, USA), IPDI (isophorone diisocyanate, from Evonik, Marl, Germany), DOA (dioctyl adipate, better named

Paper number 20069, Text pages 1 to 30, Session 3B, on 2018 NDIA-IMEMTS, event number 8550, April 23-29, 2018, Portland Oregon, USA. http://www.ndia.org/events/2018/4/23/imem

di(ethyl-hexyl) adipate, from BASF, Ludwigshafen, Germany), antioxidant Vulkanox™ BKF (from Bayer AG, Leverkusen, Germany).

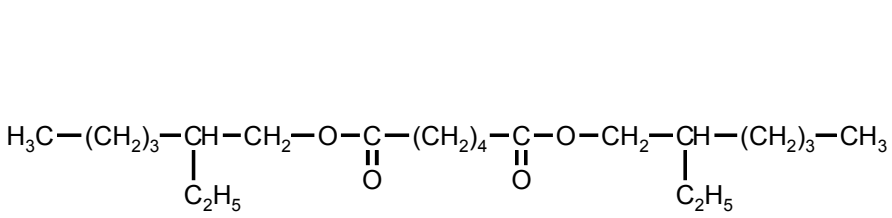

Di(ethyl-hexyl) adipate (DOA)

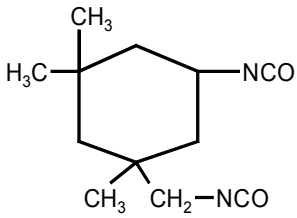

IPDI

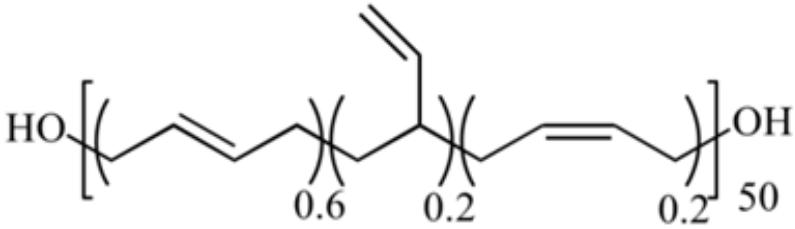

HTPB (hydroxyl terminated polybutadiene); double bond parts: cis 20%, trans 60%, vinyl 20%. The HTPB type used was HTPB R45 HTLO.

Figure 2: Ingredients of the used binder.

The three solid fillers were characterized by particle size distributions. The mean diameters are the so-called Dx50 median values, which separate the total sample in the lower and upper part, with x naming the type of particle distribution function, v = volume, m = mass, s = surface, n = number. Here the distributions with x =v are considered (normally gained from laser scattering), this means the Dv50 is the particle size in micrometer that splits the distribution with half of the total particle volume above and half of the total particle volume below this diameter. The Dv50 parameter is named the median of the volume distribution. It is with equal density for all particles equal to the mass median of a mass distribution.

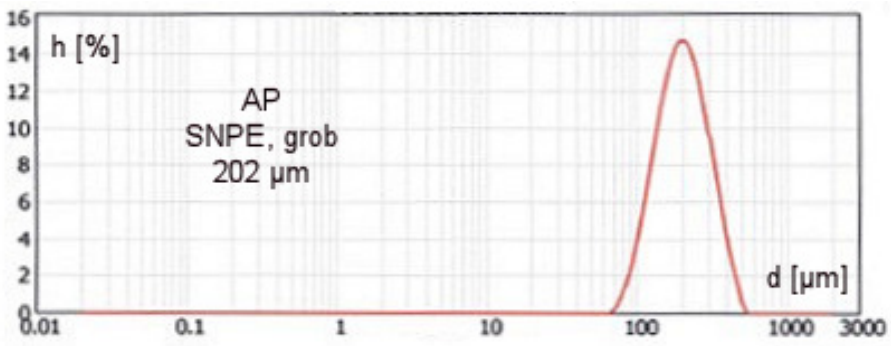

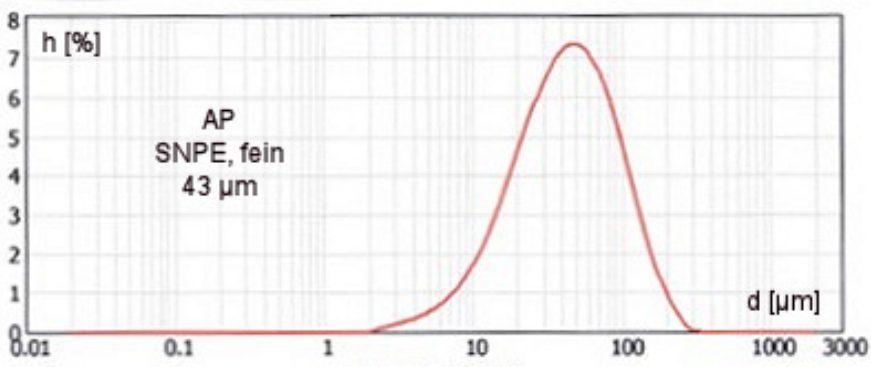

Paper number 20069, Text pages 1 to 30, Session 3B, on 2018 NDIA-IMEMTS, event number 8550, April 23-29, 2018, Portland Oregon, USA. http://www.ndia.org/events/2018/4/23/imem

Figure 3: Particle size distributions of AP, above coarse and below fine. Material obtained from former SNPE, now EURENCO, France.

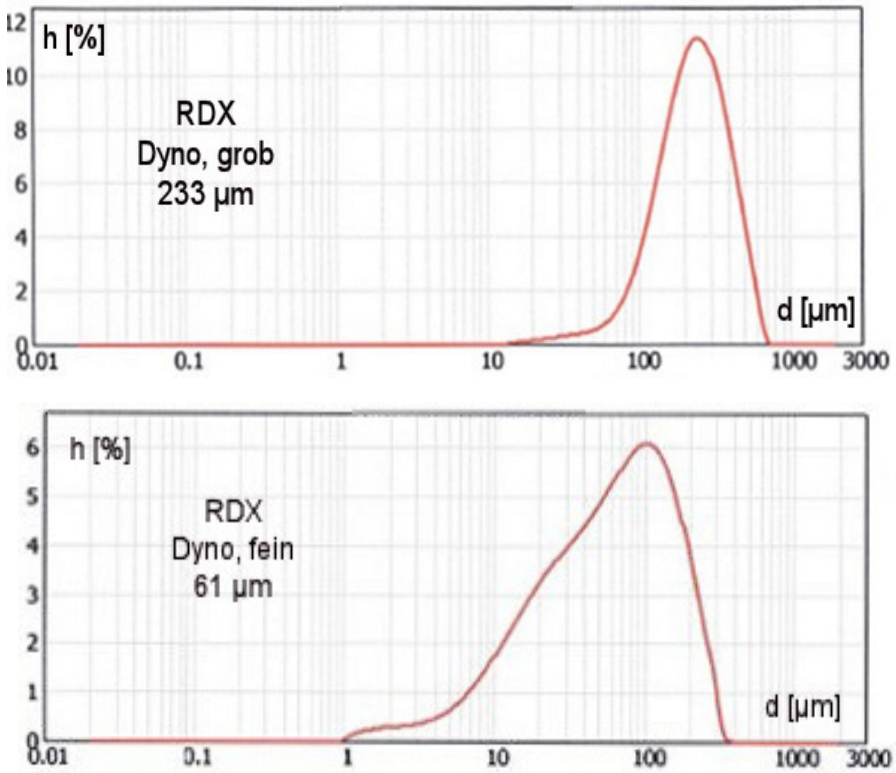

Figure 4: Particle size distributions of RDX, above coarse and below fine Material obtained from former Dyno, Norway, now Chemring.

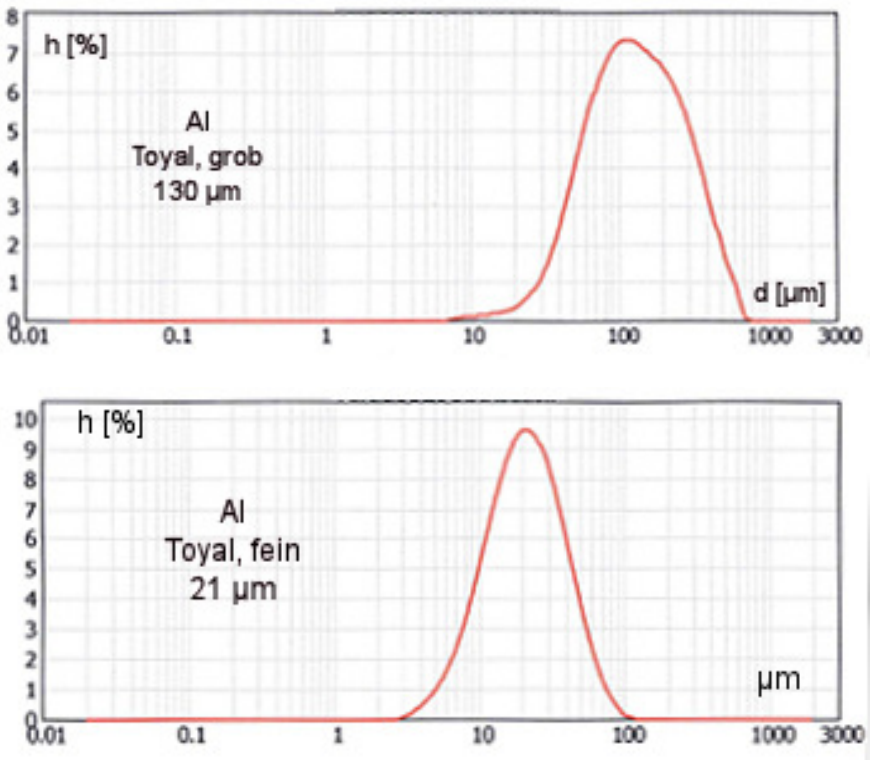

Figure 5: Particle size distributions of AL powder, above coarse and below fine. Material obtained from company Toyal, USA.

Paper number 20069, Text pages 1 to 30, Session 3B, on 2018 NDIA-IMEMTS, event number 8550, April 23-29, 2018, Portland Oregon, USA. http://www.ndia.org/events/2018/4/23/imem

2.2 Sample manufacturing

The composite samples were manufactured at Fraunhofer ICT in a planetary-rotary centrifugal vacuum mixer (from Thinky Corporation, Tokyo, Japan). The scheme of the manufacturing is shown in Fig. 6. No curing catalyst was used, and no bonding agents have been used with the fillers. All formulations were made with an equivalent ratio R_{eq} (NCO / OH) = 0.85. The plasticizer content was always 5 mass-% in binder.

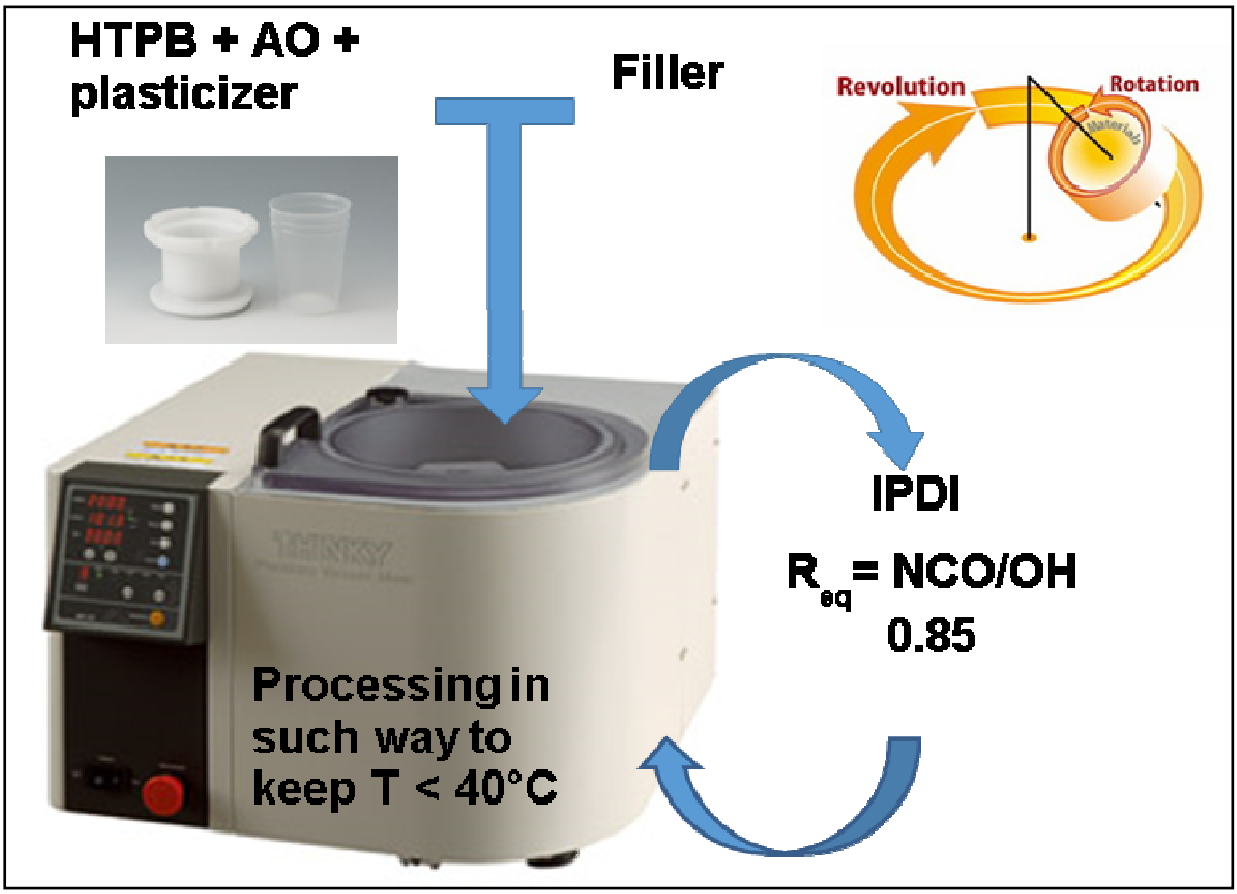

Figure 6: Scheme of the manufacturing process using a planetary-rotary mixer, of type Thinky® mixer, produced by Thinky Corporation, Tokyo, Japan.

Operational conditions were 1600 rpm rotation speed and 30 mbar = 3 kPa vacuum during the few minutes of mixing time. The temperature in the mix was kept below 40°C. Every formulation was produced in small batches and poured into a cylindrical glass recipient, sealed and cured in air at 60°C for 130 hours. The binder was protected by the addition of an antioxidant.

Shortly after the mixing the particles are homogeneously distributed all over the sample volume. However, the particles tend to sediment in the liquid binder mix in early stages of the curing process, when the viscosity is not yet high. This problem is even more critical with samples with lower amounts of solid loading, as with 20 and 40 mass-%. Thus, in order to keep the fillers homogeneously distributed during the curing process a special turning device was manufactured at Fraunhofer ICT and installed inside the curing oven, see Fig. 7, 8, 9. The turning machine provides a rectangular frame for mounting the samples within a standard laboratory circulation oven of type UFE500 from company Memmert (Germany). The frame is rotated not permanently to avoid concentration gradients of filler particles due to inertia forces. It is rotated

stepwise by 180 degrees, controlled by encapsulated, low-voltage magnetic switches. A belt drive in combination with a screw wheel transmission is powered by a brushless AC-motor. An additional transmission is necessary for suppressing so-called rattle-effects. The switches and the motor are connected to a programmable electronic circuit, which allows controlling the rotation speed and the holding time. The circuit is equipped with a mechanical counter to monitor the number of rotation cycles, useful for instance in case of failures in power network.

After curing, the glass bottles were broken and the DMA samples cut from the middle of the cured composite. In this way surface effects induced from the interface glass –binder or binder with residual air were circumvented.

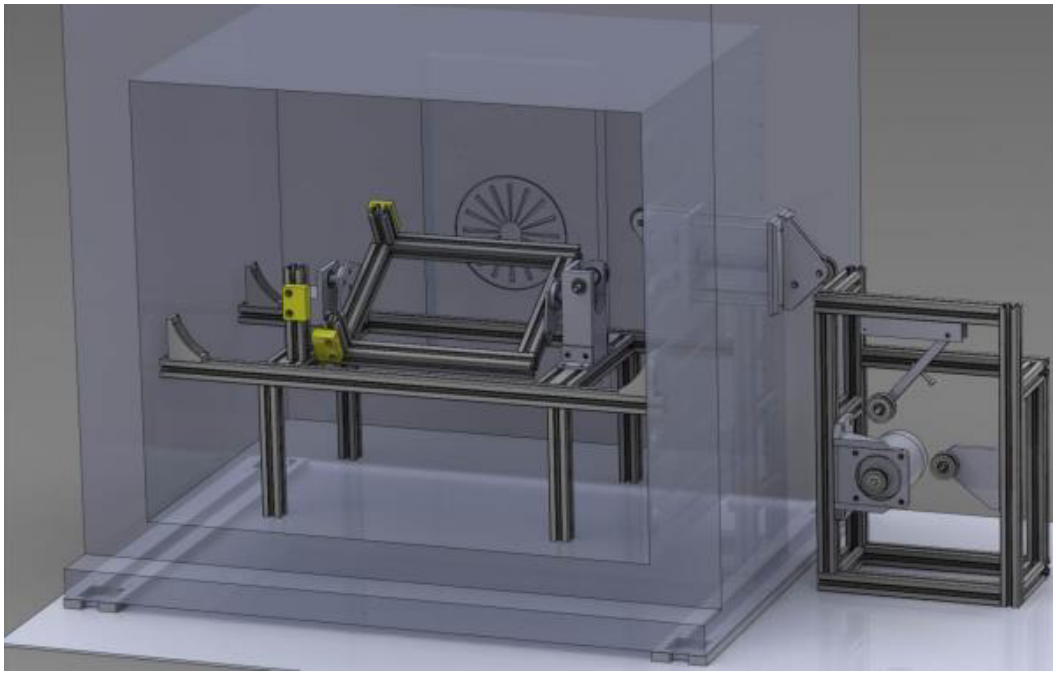

Figure 7: Construction photograph of the turning device mounted inside an air circulation oven and driven by an electromotor with stepping gear system.

Figure 8: Real photograph of the turning device inside the oven with mounted samples in small glass bottles.

Paper number 20069, Text pages 1 to 30, Session 3B, on 2018 NDIA-IMEMTS, event number 8550, April 23-29, 2018, Portland Oregon, USA. http://www.ndia.org/events/2018/4/23/imem

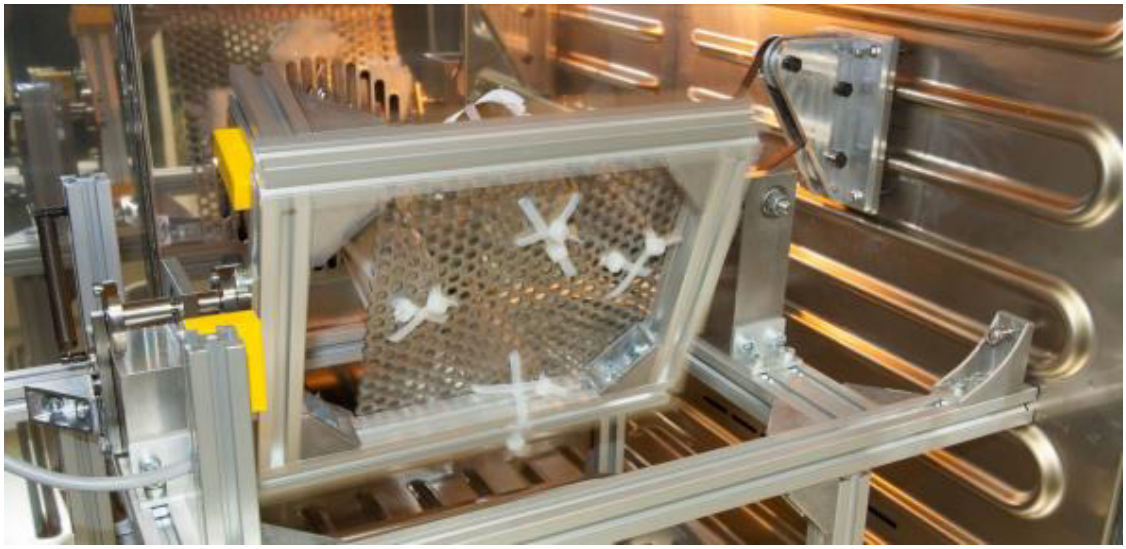

Figure 9: Real photograph of the turning device inside the oven with mounted samples in small glass bottles, indicating step-wise turning by 180°.

2.3 Characterization methods

2.3.1 X-ray (Röntgen)-Computer Tomography (X-CT)

Using a computer tomography instrumentation of type Micro-CT in-vivo Skyscan 1076 of company Bruker, Germany, the cured samples were tested, whether the distribution of the solid fillers was homogeneous. The maximum peak voltage of the X-ray is 100 kV with a maximum power of 10 W. It has a Tungsten reflection target and a focal spot of 5 µm. The detection system consists of a 8000 x 8000 large megapixel X-ray camera. A micro-focus X-ray source illuminates the object and the planar X-ray detector collects magnified projection images. Based on hundreds of angular views acquired while the object rotates, a computer synthesizes a stack of virtual cross section slices through the object. After the acquisition of the projection images, the reconstruction was done using a modified Feldkamp cone beam algorithm. Finally, the 2D cross-sectional images of the sample were obtained in consecutive slices throughout the object. Also 3D images can be constructed.

2.3.2 Scanning Electron Microscopy (SEM)

Scanning electron microscopy of type Supra 55VP, manufactured by company ZEISS, Germany was used to characterize the surfaces of the particles with regard to their roughness or smoothness.

2.3.3 Dynamic Mechanical Analysis (DMA)

Dynamic mechanical analysis measurements in torsion mode were carried out with a DMA of type ARES™ (Advanced Rheometric Expansion System) manufactured by the former Rheometric Business Unit of Rheometric Scientific, Inc. (this BU now belongs to TA Instruments, New Castle, DE, USA). The following parameters were determined: storage shear modulus G', loss shear modulus G'', loss factor tanδ = G''/G' as well as the phase angle δ and the torque. Measurements were performed in torsion mode from -100°C to +70°C, with heating steps of 1°C/min and soak time of 28s. At -100°C a pre-strain sweep test was performed to determine the value of the strain control, in order to stay in the linear viscoelastic region during the measurements. At each temperature step, the samples were measured at four sinusoidal

deformation frequencies, here 0.1; 1.0; 10 and 30 Hz. The geometrical dimensions of the rectangular samples were about 40 mm in length, 10 mm in width and 5 mm in thickness. In the cases where the material was too soft, as with pure binder and binder with 20 and 40 mass-% of filler, the signal scattered at higher temperatures and a second strain sweep was necessary at -40°C to determine a higher second strain control to be used up to +70°C.

The temperatures of the two evident maxima in the loss factor curve tanδ(T) = G''(T)/G'(T) of the HTPB-IPDI binder were determined by using fits of polynomials of degree 3 around the maxima and calculating the temperatures connected with the maxima. These temperatures are named $T_{g,DMA}$ and represent glass-rubber transitions (GRT) in the corresponding binder parts. The temperatures at maxima of the loss factor curve are seen as the representative transition temperatures, because around these temperatures the necessary molecular reorientations (= transitions in molecular arrangements) to come from glassy to rubbery state (and vice versa) have the highest 'intensity' or activity. The assignments to these both evident peaks is T_g^{unr} (unrestricted binder mobility) and T_g^{res} (restricted binder mobility). Unrestricted binder regions are parts of the inter-cross-link chain segments, which are not restricted in mobility by the fillers, as sterically-geometrically and by energetic interaction, and also not by other mobility hindrances, as they occur in the cross-link ranges of the binder. These binder parts in cross-link volume elements with restricted mobility are one origin for the second apparent maximum in the loss factor curve, situated at higher temperatures than the first peak maximum, what is caused by the transition of the unrestricted binder parts.

2.3.4 Exponentially Modified Gauss distribution (EMG distribution)

The peaks of the loss factor curves correspond with the different mobility of the polymer chains of the elastomer network. An objective is to identify and quantify the corresponding binder parts. For this, a suitable description has to be applied. The so-called EMG functions have shown to provide with the looked for parameters [5,6,7,8,9]. The EMG function is a convolution between a Gauss distribution function, Eq.(1) and an exponential decay function, Eq.(2), resulting in Eq.(3).

$$f_G(T) = \frac{A}{w \cdot \sqrt{2\pi}} \cdot \exp\left[-0.5 \cdot \left(\frac{T - Tc}{w} \right)^2 \right] \tag{1}$$

$$f_E(T) = \exp\left(-\frac{T}{\tau} \right) \tag{2}$$

$$\tan\delta_{BLC} = td_0 + \frac{A}{\tau} \cdot \frac{1}{2} \cdot \exp\left[0.5 \cdot \left(\frac{w}{\tau} \right)^2 - \frac{T - Tc}{\tau} \right] \cdot \left\{ 1 - \mathrm{erf}\left[-\frac{1}{\sqrt{2}} \left(\frac{T - Tc}{w} - \frac{w}{\tau} \right) \right] \right\} \tag{3}$$

T measurement temperature, in [°C];
$\tan\delta_{BLC}$ value of loss factor as function of T after BLC (baseline correction), in [-];
A peak area of the EMG peak, also equivalent to the area of the corresponding Gauss peak alone, in [°C];
w half peak width at half height of only the Gauss part, in [°C];
Tc temperature at peak maxima in the Gauss part of EMG (not the peak maxima of EMG), in [°C];
τ relaxation parameter in exponential part of EMG, also named To, in [°C];
td_0 to consider an eventually residual offset in tanδ data, in [-];
erf error function.

Meanwhile it was several times found and confirmed that the total loss factor curve of an HTPB-IPDI binder needs three EMG functions for full description [2,3,4,5,6], see Eq.(4).

$$\tan\delta_{BLC} = td_0 + \sum_{i=1}^{N} \frac{A_i}{\tau_i} \cdot \frac{1}{2} \cdot \exp\left[0.5 \cdot \left(\frac{w_i}{\tau_i}\right)^2 - \frac{T - Tc_i}{\tau_i}\right] \cdot \left\{1 - \mathrm{erf}\left[-\frac{1}{\sqrt{2}}\left(\frac{T - Tc_i}{w_i} - \frac{w_i}{\tau_i}\right)\right]\right\} \quad (4)$$

Each EMG function comprises four parameters. In spite of the high number of parameters, the fit is mostly easy to perform and is unique, because the structures of the peaks and the equations limit the possibilities for the fit [2]. To apply the EMG description the loss factor curves must be baseline corrected, see [6]. Figure 10 presents an example of modelling the loss factor curve; the three single EMG (peak 1, 2, 3) and the total EMG are shown.

There are some rules for the change of the parameters A, Tc and τ (To)

> Peak areas A_i:

Reduction of A is caused by:
(1) – Hindrance of mobility
(2) – increase in storage shear modulus G' or increase in stiffness or in rigidity
(3) – increase in cross-linking
(4) – loss of plasticizer

> Peak temperature Tc_i of the Gauss curve

This temperature can be considered as glass-rubber-transition temperature of the relaxation free transition, means the transition without an exponential decay part. It changes by interactions, which restrict the mobility.

> Relaxation parameter τ_i

The more influence the exponential part the larger is τ_i or To and the more scewed is the EMG curve.

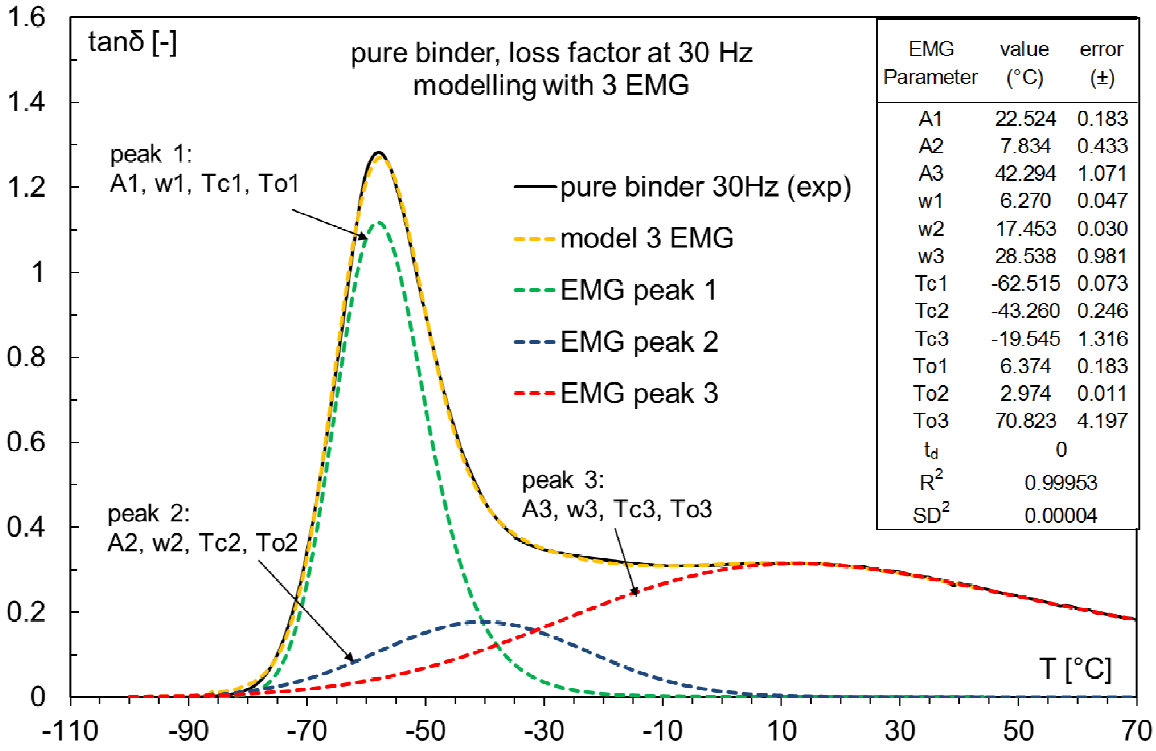

EMG Parameter	value (°C)	error (±)
A1	22.524	0.183
A2	7.834	0.433
A3	42.294	1.071
w1	6.270	0.047
w2	17.453	0.030
w3	28.538	0.981
Tc1	-62.515	0.073
Tc2	-43.260	0.246
Tc3	-19.545	1.316
To1	6.374	0.183
To2	2.974	0.011
To3	70.823	4.197
t_d	0	
R^2	0.99953	
SD^2	0.00004	

Figure 10: Example of description with three EMG function of baseline corrected loss factor curve of the HTPB-IPDI binder (with plasticizer) used here. Deformation frequency was 30 Hz.

Peak 1 describes the mobility unrestricted binder part, peak3 the mobility restricted binder part (in cross-link volume elements) and peak 2 is caused by intermediate restricted binder parts.

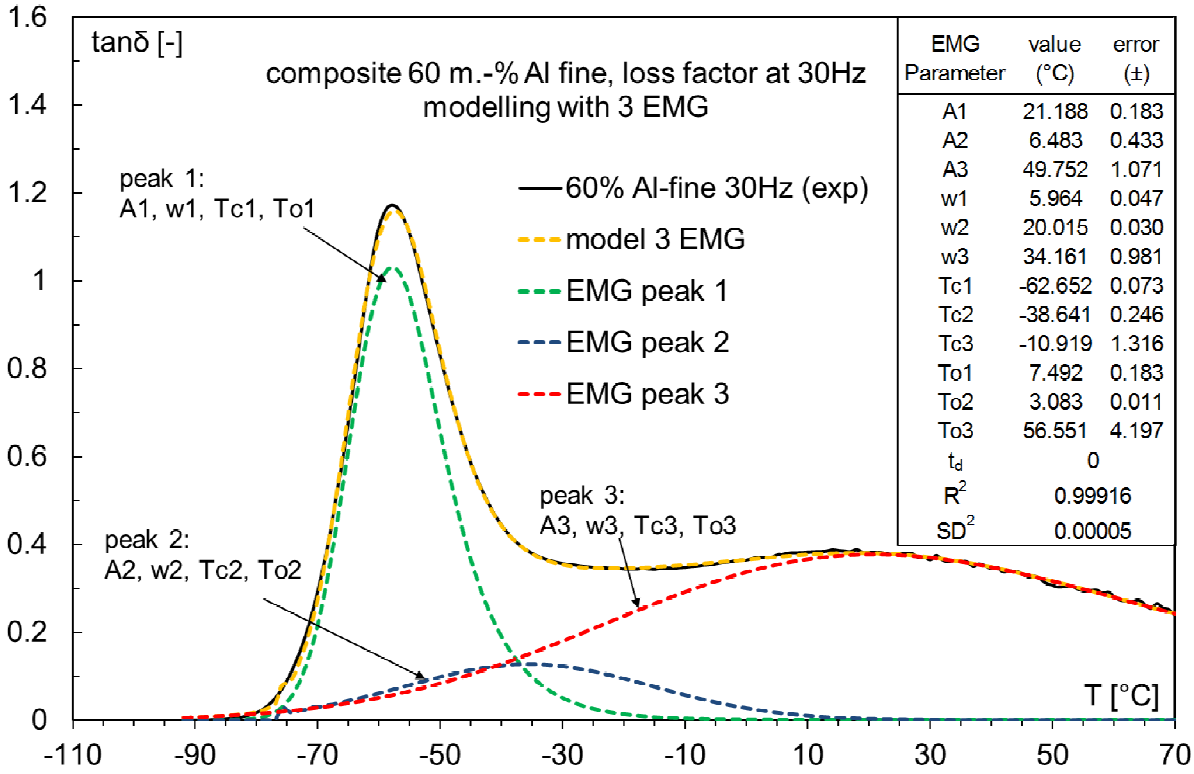

Figure 11: Description with three EMG function of the baseline corrected loss factor curve of HTPB-IPDI binder (with plasticizer) filled with 60 mass-% fine Al. Deformation frequency was 30 Hz.

Figure 11 shows the description with three EMG functions of the baseline corrected loss factor curve of HTPB-IPDI binder filled with 60 mass-% fine Al. By comparison with Figure 10, the binder alone, the following effects can be stated: The main peak 1 is a bit lowered in intensity, but the shape is not much influenced by relaxation, the To values are similar and the maximum is not shifted. This means the changes are caused just by geometrical hindrance from the Al particles. The peak 3 has increased in intensity and is more clearly established. Further on the maximum of the apparent peak has shifted from about +11°C to + 15°C (binder + Al). The corresponding Gauss peaks have the maxima at -19.5°C and -10.9°C. Because of the large To_3 values, the actual EMG peak shifts massively to higher temperatures. This means Al particles interfere strongly with the binder parts restricted already in mobility. There in this binder part they cause more mobility restrictions indicated by the shift of the maximum temperature of Al filled binder to higher values. This is not contradicting the increase in intensity of this peak, because now more parts of the binder are involved, which increases intensity of this peak. In addition, as already said, the first peak is not shifted or only very minor, means here the hindrance is only sterically and not much interaction energy caused.

3. Results and Discussion

3.1 Uniformness of filler distribution in the cured binder

In Fig 12a and 12b, the sample with 20 mass-% of coarse AP is shown as an example of how the particles stayed homogeneously distributed in the elastomers after curing when applying the turning machine. The 3D image obtained with Bruker Micro-CT X-ray Skyscan is shown in

Figure 12b, and it demonstrates the uniformness of the distribution of the AP particles, given in grey colour. The binder itself is not visible because of contrast adjustment.

(a)

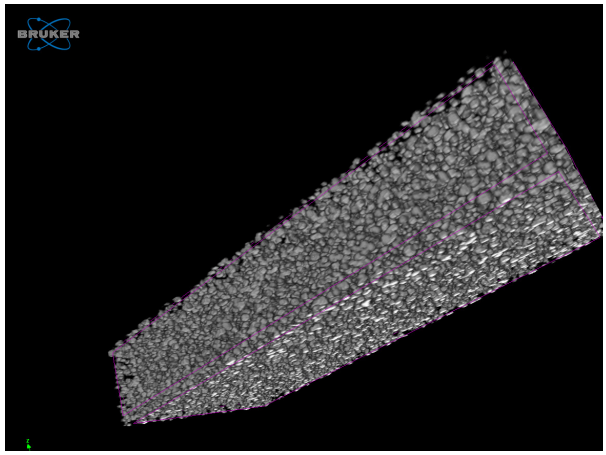

(b)

Figure 12: Images from a DMA sample with 20 mass-% AP. (a) a normal optical photograph and (b) a 3D image evaluated with the Bruker Micro-CT X-ray Skyscan, showing the AP particles in grey (binder cannot be seen).

3.2 DMA measurements

The Figures 13a to 13c show an overview of the loss factor curves of the samples with 60 mass-% of coarse AP, 60 mass-% of coarse RDX and 60 mass-% of fine Al at the deformation frequencies of 0.1 to 30 Hz. In Figures 14a to 14c, the elastic (storage) shear modulus G' and the (viscous) loss shear modulus G" are presented for all the samples, tested at the deformation frequency of 10 Hz.

The molecular rearrangements during glass-rubber transition enhance the thermo-mechanical energy loss inside the polymer. Therefore, the loss shear modulus increases. During glass-rubber transition, when the molecules are stimulated to pass the threshold of energy, long range chain mobility takes place along the segments and the loss factor is at its maximum. By increasing the deformation frequency in DMA, the chains have less time to move and rearrange in order to accommodate the mechanical energy. When heating up the samples from very low temperatures, the energy elastic state is retained longer, up to higher temperatures. This effect is also named strain rate hardening of the material.

Despite having less effect on the first peak, the Al addition imparts more intensity to tanδ of the second peak; and it is shifted to higher temperatures (see T_g^{res} values of 60 m.-% filled samples in Table 2). However, a distinguishable change in the first peak with the addition of AP and RDX in comparison to Al could be related with volumetric effects. The densities of AP and RDX are 1.95 g/cm^3 and 1.82 g/cm^3, respectively, whereas Al has 2.7 g/cm^3. The use of an equal mass results in a higher occupied volume by the particles in composites with AP and RDX, imparting more geometrical hindrance to chain mobility than by the Al particles which are less in number. Table 1 shows the data.

Table 1: Connection between mass-% and vol-%

	density in g/cm^3	mass-%	volume in 100g [cm^3]	total volume of 100g [cm^3]	vol.-%	degree of volume filling relative to AP

AP	1.95	60	30.77	73.78	41.71	1
RDX	1.816	60	33.04	76.05	43.45	1.04
Al	2.7	60	22.22	65.23	34.06	0.82
HTPB-IPDI-DOA	0.93	40	43.01	-	-	-

On the other hand, Al filled samples present a higher intensity on the second peak, which might originate from higher filler-binder interactions. By increasing the amount of AP and RDX particles, the T_g^{unr} is shifted slightly to higher temperatures. And it decreased considerably the tanδ intensity of the first peak especially at higher deformation frequencies.

Before the transition, G' and G" are very similar for the composites. Only G' of samples with 60 mass-% is significantly higher. Increasing the amount of AP and RDX particles enhances G' and G", although with AP this happens mainly after T_g^{unr}. Al produces this effect more pronounced at lower temperatures. After transition the differences increase, and it is notable that the increase in solid filler content in the composites increases both G' and G". Storage modulus increase is related with a reinforcement of the material, whereas loss modulus increase with increasing solid fillers in composites is known to be caused by an enhanced internal friction in dynamic mechanical loading experiments [8,22]. Regarding particle sizes, the use of fine AP and fine RDX incremented G' more than G".

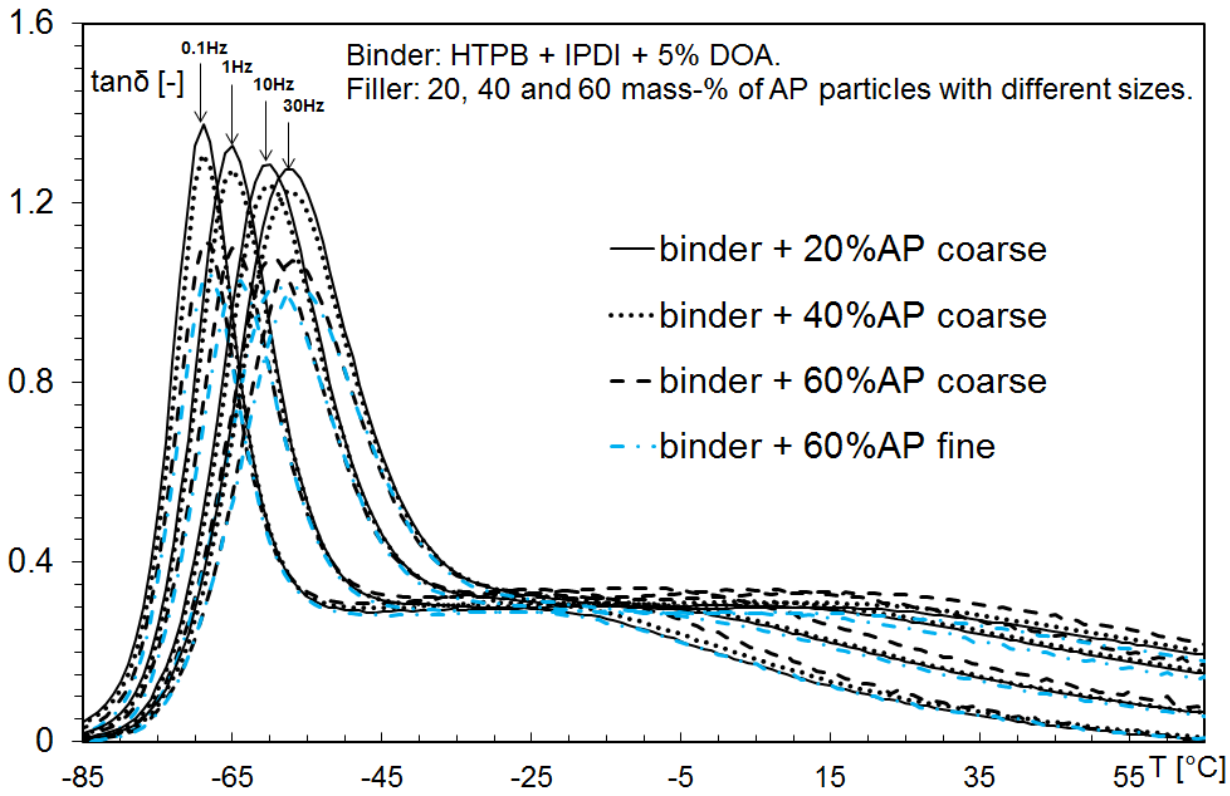

Figure 13a: Deformation frequency dependence of the loss factor curve of composites samples with 20, 40 and 60 mass-% of AP coarse and 60 mass-% of AP fine particles.

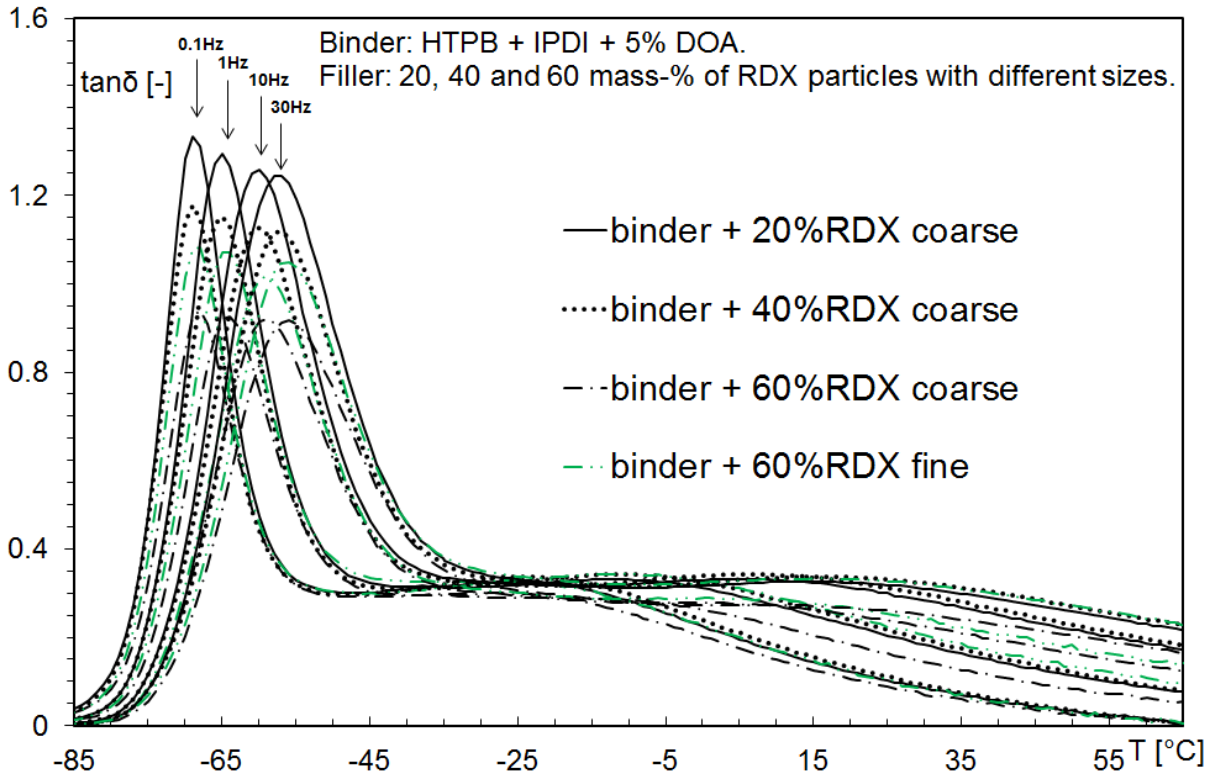

Figure 13b: Deformation frequency dependence of the loss factor curve of composites samples with 20, 40 and 60 mass-% of RDX coarse and 60 mass-% of RDX fine particles.

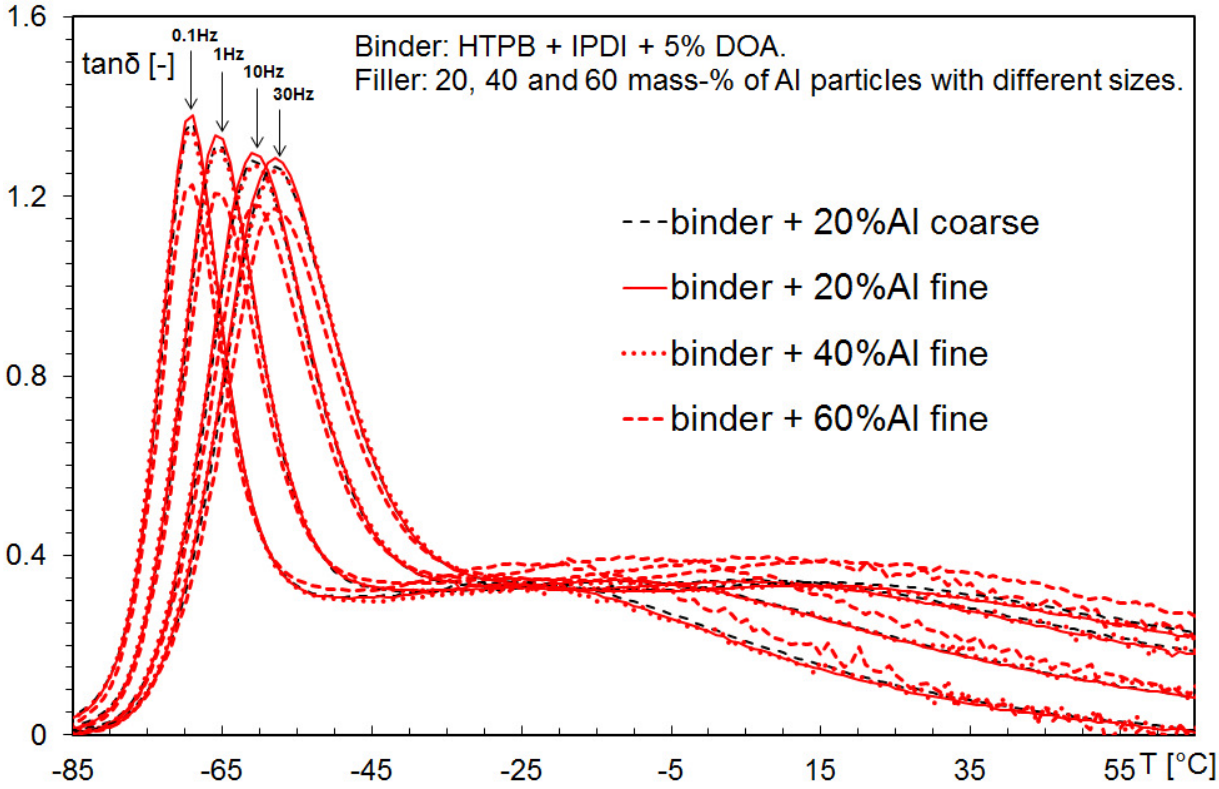

Figure 13c: Deformation frequency dependence of the loss factor curve of composites samples with 20, 40 and 60 mass-% Al fine and 60 mass-% Al coarse particles.

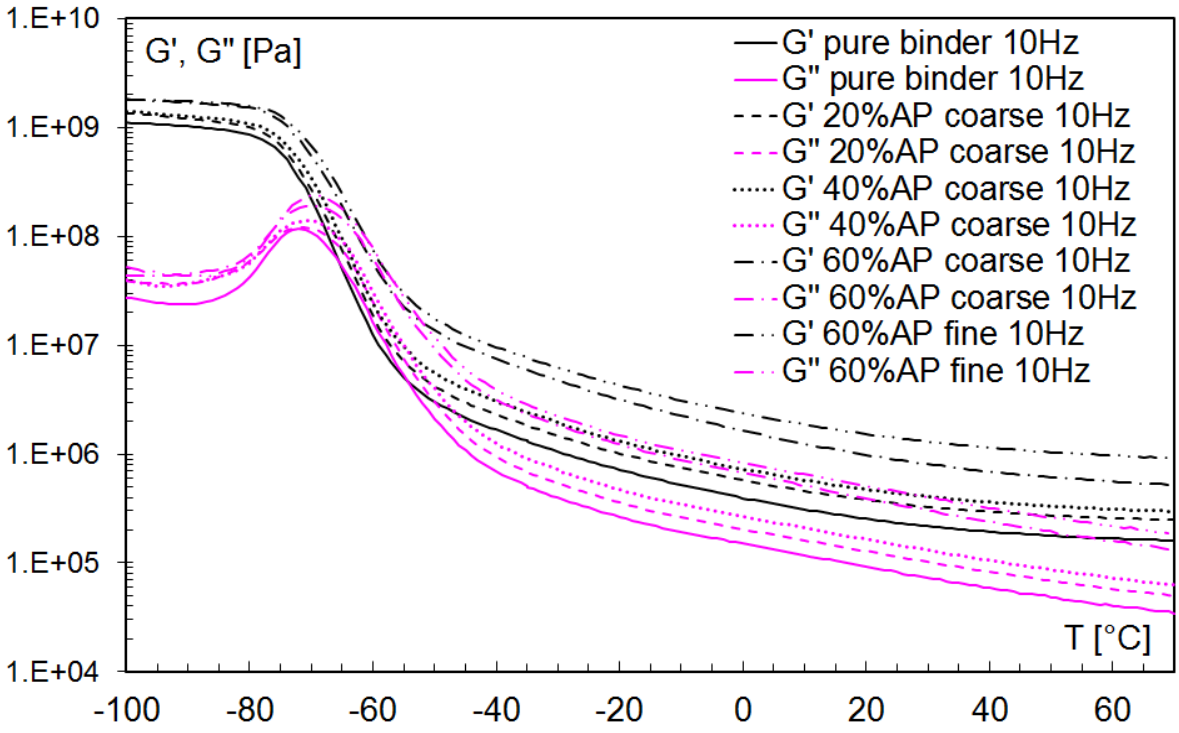

Figure 14a: G' and G" curves of samples tested at 10 Hz deformation frequency of applied strain in torsion mode DMA. Samples consisting of pure binder and binder with increasing amount (20, 40 and 60 mass-%) of coarse AP particles and 60 mass-% of fine AP.

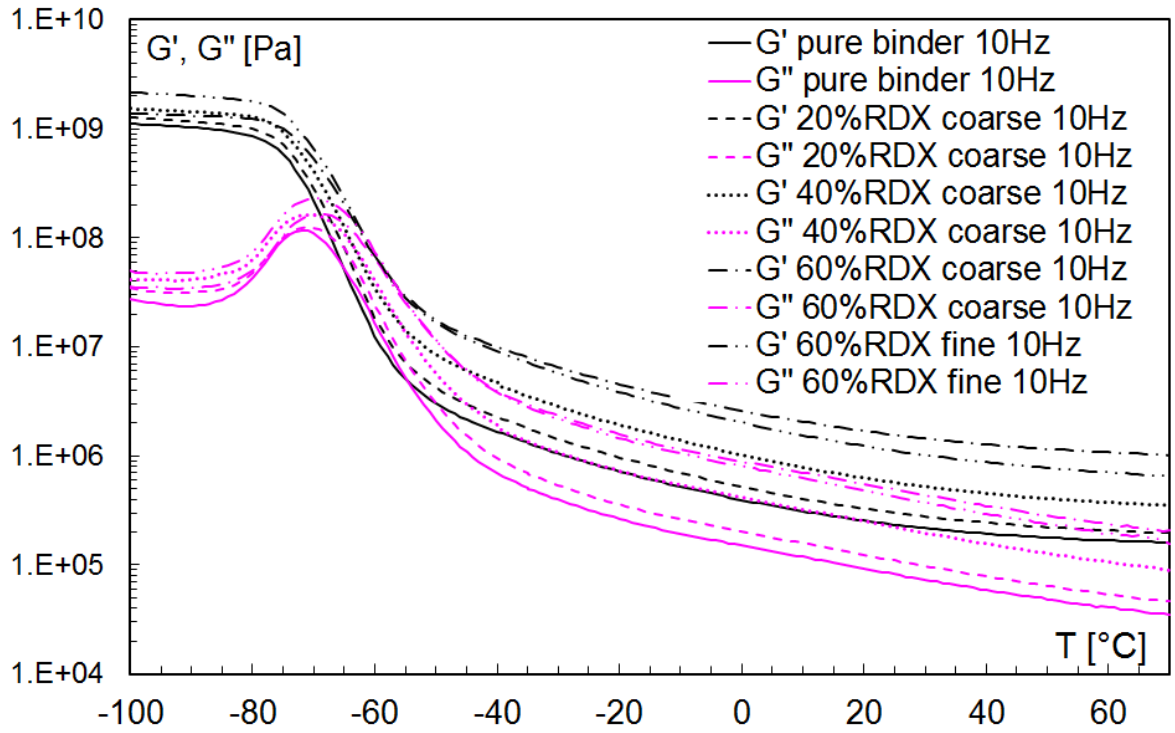

Figure 14b: G' and G" curves of samples tested at 10 Hz deformation frequency of applied strain in torsion mode DMA. Samples consisting of pure binder and binder with increasing amount (20, 40 and 60 mass-%) of coarse RDX particles and 60 mass-% of fine RDX.

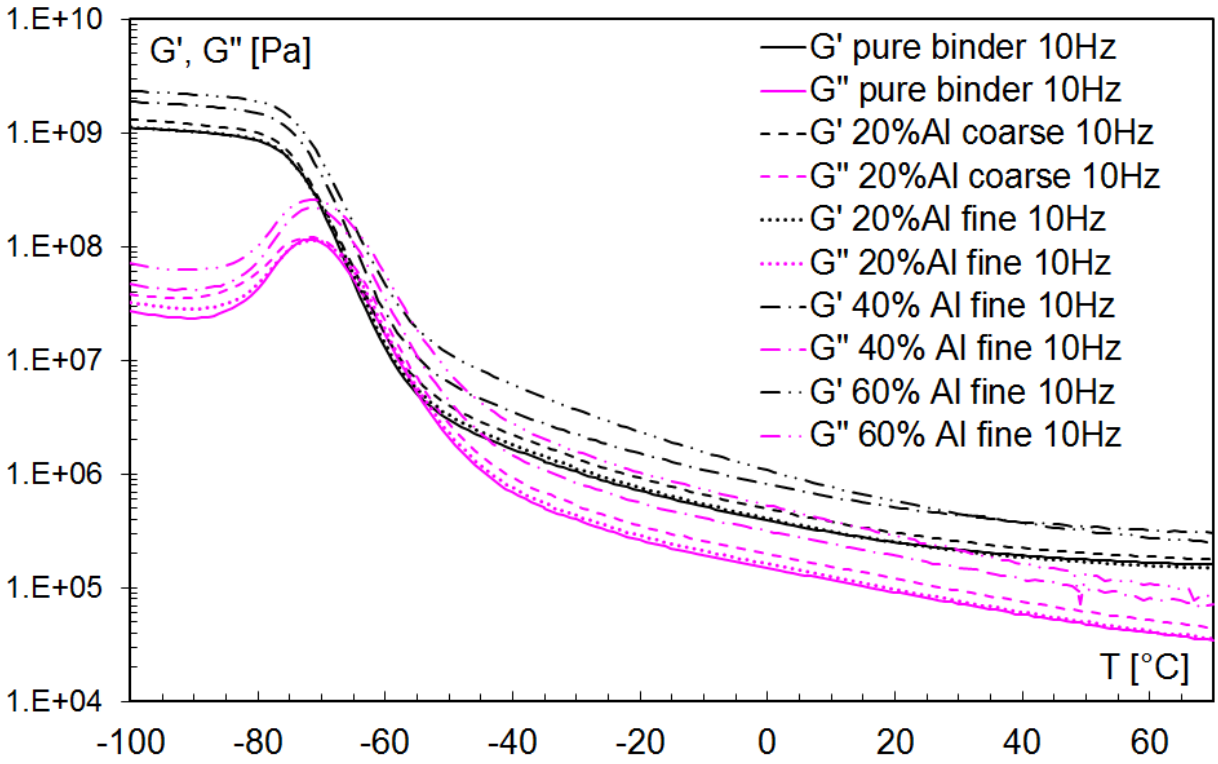

Figure 14c: G' and G" curves of samples tested at 10 Hz deformation frequency of applied strain in torsion mode DMA. Samples consisting of binder and binder with increasing amount (20, 40 and 60 mass-%) of fine aluminum particles and of 20 mass-% coarse Al.

3.3 EMG modelling of loss factor data

The quantification of the effects caused by energetic interaction and by the amount of each filler on the loss factor curve is possible with the use of exponentially modified Gauss (EMG) distribution functions. In Fig. 10 and Fig. 11, each three EMG functions are used to describe the total tanδ data of the pure binder and of the composite filled with 60 mass-% of fine Al particles. This was done for all samples at all deformation frequencies. The parameters obtained for the samples filled with 60 mass-% fine and coarse particles are presented in Table 2.

Figure 15 shows the loss factor curves and the EMG functions of the samples filled with 60 m.-% of fine RDX at different frequencies of applied strain and their EMG modelling. It shows the systematic development with deformation frequency of the total loss factor curve and of the three EMG functions used at each frequency. In Fig 16a to Fig. 16d the changes with deformation frequency of the four parameters Ai, Tci, wi and Toi of the three EMG peak are presented graphically. There is always an increase with frequency. To note: the changes for peak 3. This peak is always more sensitive to deformation rate than the other two.

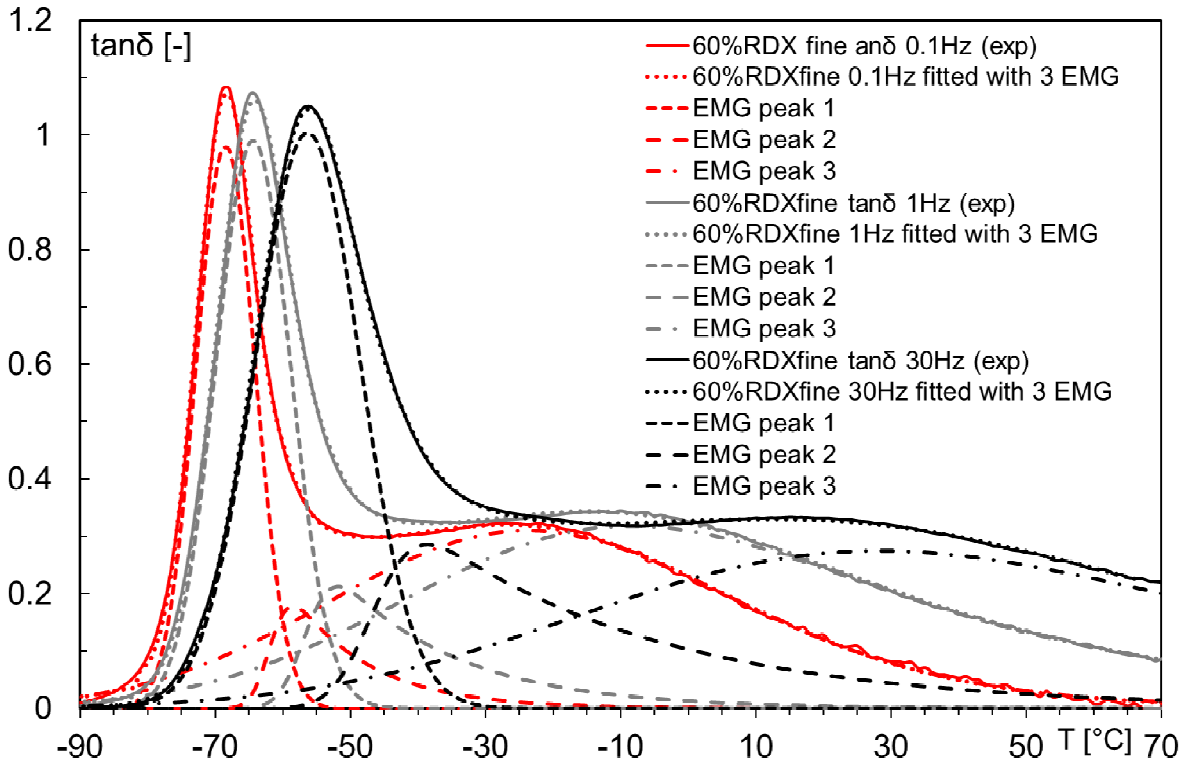

Figure 15: Description of loss factor curves with 3 EMG functions, of the sample with 60 m.-% of fine RDX. Torsion DMA in 0.1, 1 and 30Hz. The indication (exp) means experimental data.

Table 2: Values of EMG parameters of samples with 60 mass-% coarse and fine particles, in comparison with the pure binder. Data given at all four applied deformation frequencies f [Hz]. The unit of all quantities is °C, also the one of the areas.

	pure binder				60 m.% AP coarse				60 m.% AP fine				60 m.% RDX coarse				60 m.% RDX fine				60 m.% Al fine			
f [Hz]	**0.1**	**1**	**10**	**30**	**0.1**	**1**	**10**	**30**	**0.1**	**1**	**10**	**30**	**0.1**	**1**	**10**	**30**	**0.1**	**1**	**10**	**30**	**0.1**	**1**	**10**	**30**
A_1	13.3	16.7	20.3	22.5	10.8	13.5	16.2	18.0	11.0	13.9	17.0	22.5	9.7	12.1	16.2	19.2	10.8	13.7	17.4	19.4	13.4	14.9	17.7	21.2
A_2	2.6	5.6	7.2	7.8	2.8	4.8	8.2	8.3	3.7	7.9	7.6	6.7	3.3	6.3	7.3	6.1	3.0	5.4	10.1	13.4	2.6	5.2	7.5	6.5
A_3	24.8	29.0	39.0	42.3	25.2	30.9	38.7	45.8	19.9	21.3	31.3	34.1	21.3	22.9	28.6	33.5	23.9	32.5	35.6	37.4	25.4	35.6	48.2	49.8
$\sum A_i$	40.8	51.3	66.5	72.7	38.8	49.3	63.2	72.2	34.5	43.1	56.0	63.3	34.3	41.2	52.2	58.8	37.7	51.6	63.1	70.2	41.4	55.7	73.4	77.4
w_1	4.2	5.2	5.6	6.3	4.3	5.2	5.6	6.3	4.5	5.5	6.1	6.7	4.5	5.5	6.0	6.7	4.3	5.4	6.8	7.6	4.2	5.2	5.1	6.0
w_2	2.0	2.7	16.4	17.5	2.1	2.8	17.0	17.5	2.3	3.1	16.5	6.6	2.2	3.1	17.4	17.3	2.2	3.1	4.1	4.8	1.7	2.9	21.1	20.0
w_3	25.3	26.3	26.7	28.5	26.8	27.7	25.5	28.1	24.7	25.6	23.9	30.6	25.9	27.0	23.8	27.4	26.2	26.7	31.6	34.6	25.8	27.0	30.1	34.2
Tc_1	-70	-66	-65	-63	-69	-66	-64	-61	-69	-65	-63	-65	-69	-65	-64	-62	-69	-65	-61	-58	-70	-66	-65	-63
Tc_2	-63	-58	-46	-43	-62	-57	-46	-42	-61	-56	-43	-57	-61	-57	-41	-34	-62	-57	-50	-47	-63	-58	-49	-39
Tc_3	-43	-33	-23	-20	-38	-32	-20	-17	-39	-28	-19	-12	-40	-31	-18	-14	-39	-33	-16	-5	-41	-30	-20	-11
To_1	0.9	1.0	5.6	6.4	0.8	1.0	5.5	6.1	0.9	1.0	5.8	23.8	0.8	1.0	6.8	8.2	0.8	1.0	1.4	1.5	0.8	1.0	6.6	7.5
To_2	9.6	17.1	2.7	3.0	11.4	16.6	3.2	3.0	15.4	26.8	3.3	1.0	15.5	22.4	3.3	3.2	11.6	17.9	29.3	35.5	9.9	16.0	3.0	3.1
To_3	22.3	37.6	60.1	70.8	17.6	35.1	59.3	75.1	20.9	34.5	57.9	66.6	19.7	32.8	54.4	65.3	19.3	43.3	54.6	60.1	21.0	35.8	59.3	56.6

Paper number 20069, Text pages 1 to 30, Session 3B, on 2018 NDIA-IMEMTS, event number 8550, April 23-29, 2018, Portland Oregon, USA.
http://www.ndia.org/events/2018/4/23/imem

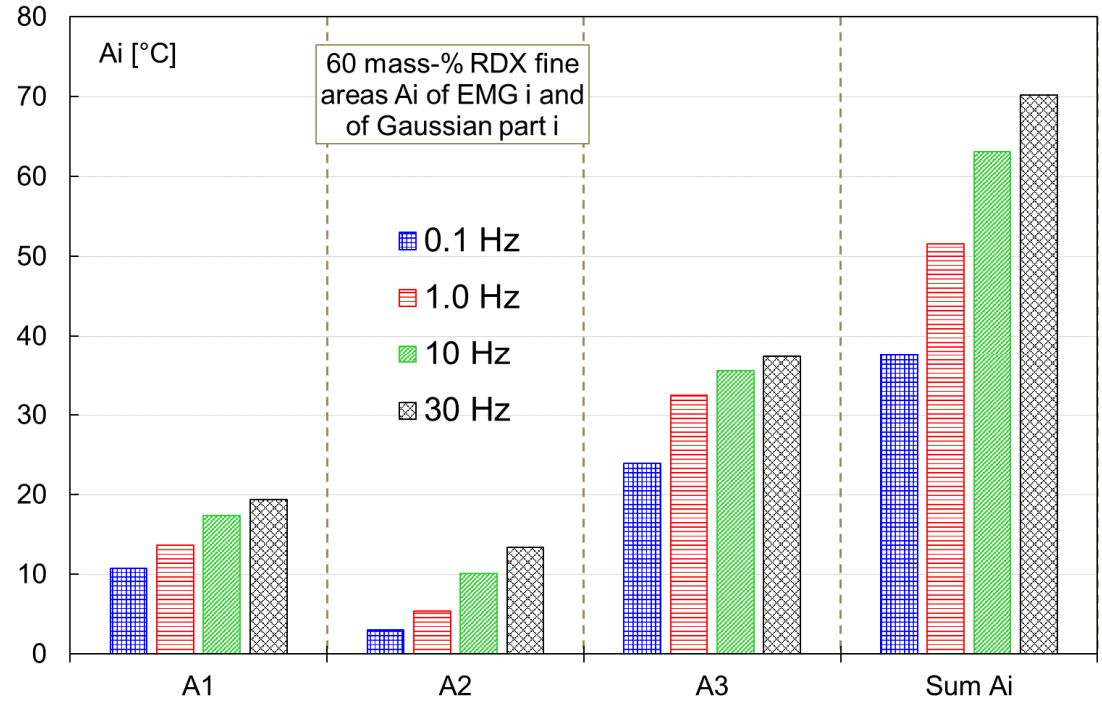

Figure 16a: Change in areas Ai of the three EMG peaks in composite HTPB-60 m.%-RDX fine with applied deformation frequency. All three areas increase with frequency. Area Ai is the same for total EMG curve and the corresponding Gauss curve.

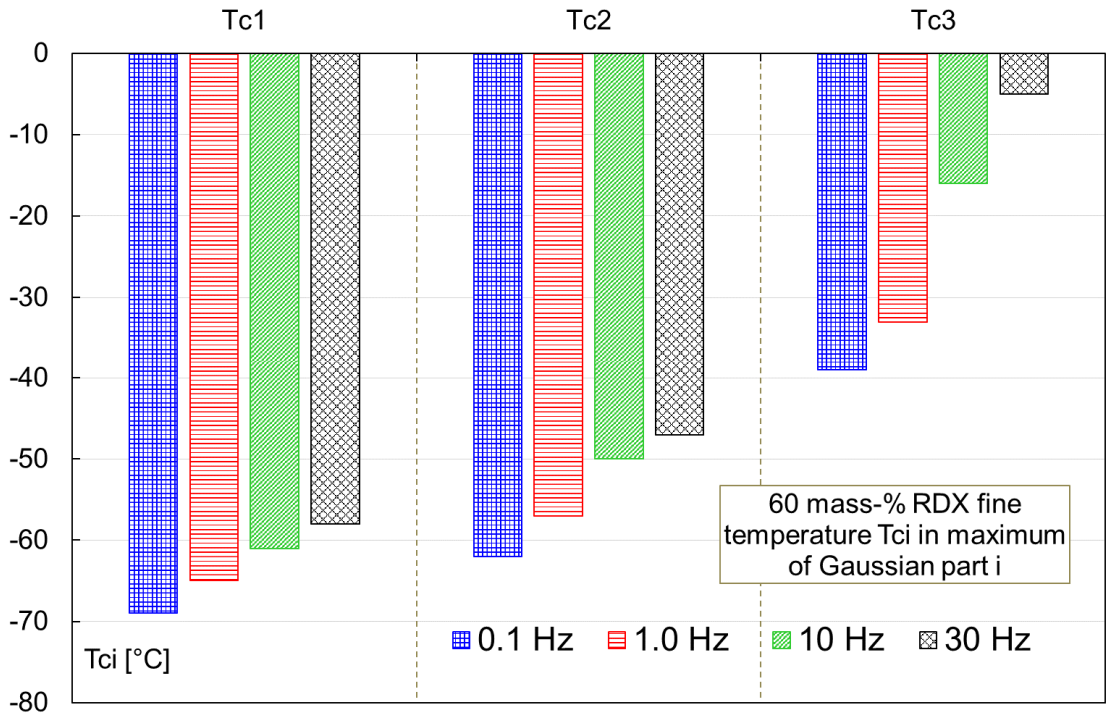

Figure 16b: Change in Gauss peak temperatures Tci of the three EMG peaks in composite HTPB-60 m.%-RDX fine with applied deformation frequency. All three temperatures are shifted to less negative values with frequency. Relatively seen is the change in Tc_3 greatest.

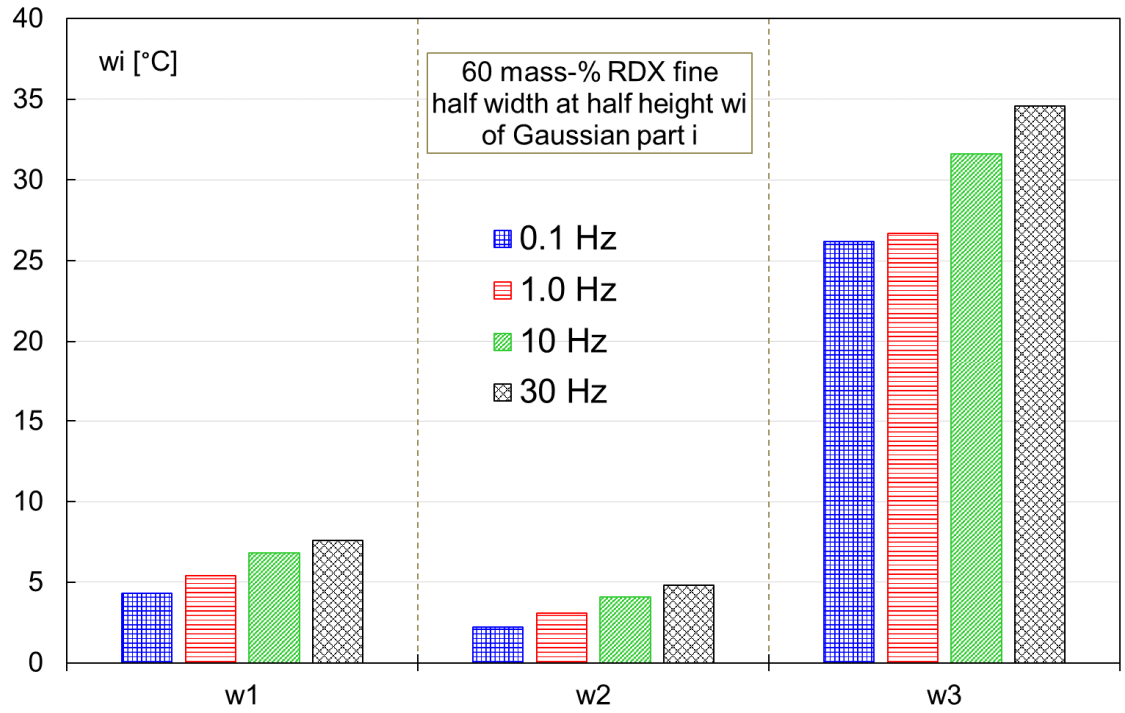

Figure 16c: Change in Gauss peak half width wi of the three EMG peaks in composite HTPB-60 m.%-RDX fine with applied deformation frequency. The half width always increases in one group with frequency. The half width of peak 3 is largest and the relative increase is pronounced.

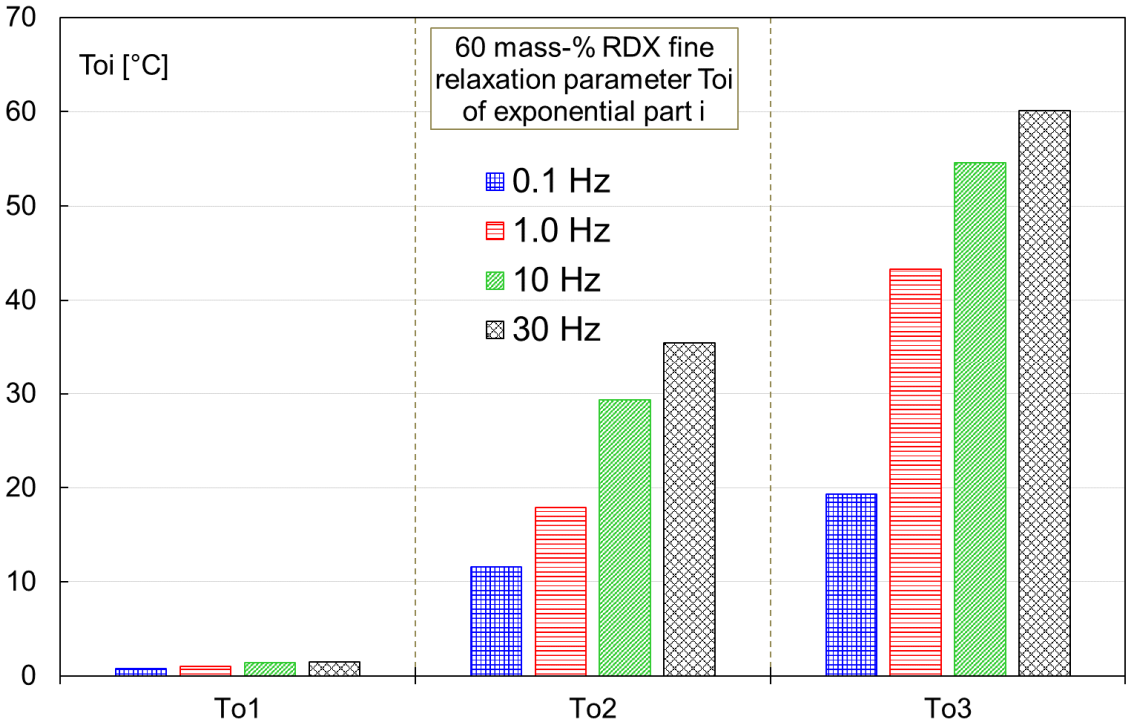

Figure 16d: Change in relaxation parameter Toi of the three EMG peaks in composite HTPB-60 m.%-RDX fine with applied deformation frequency. All three parameters increase with frequency. The parameter of peak 3 is largest and the relative increase is pronounced.

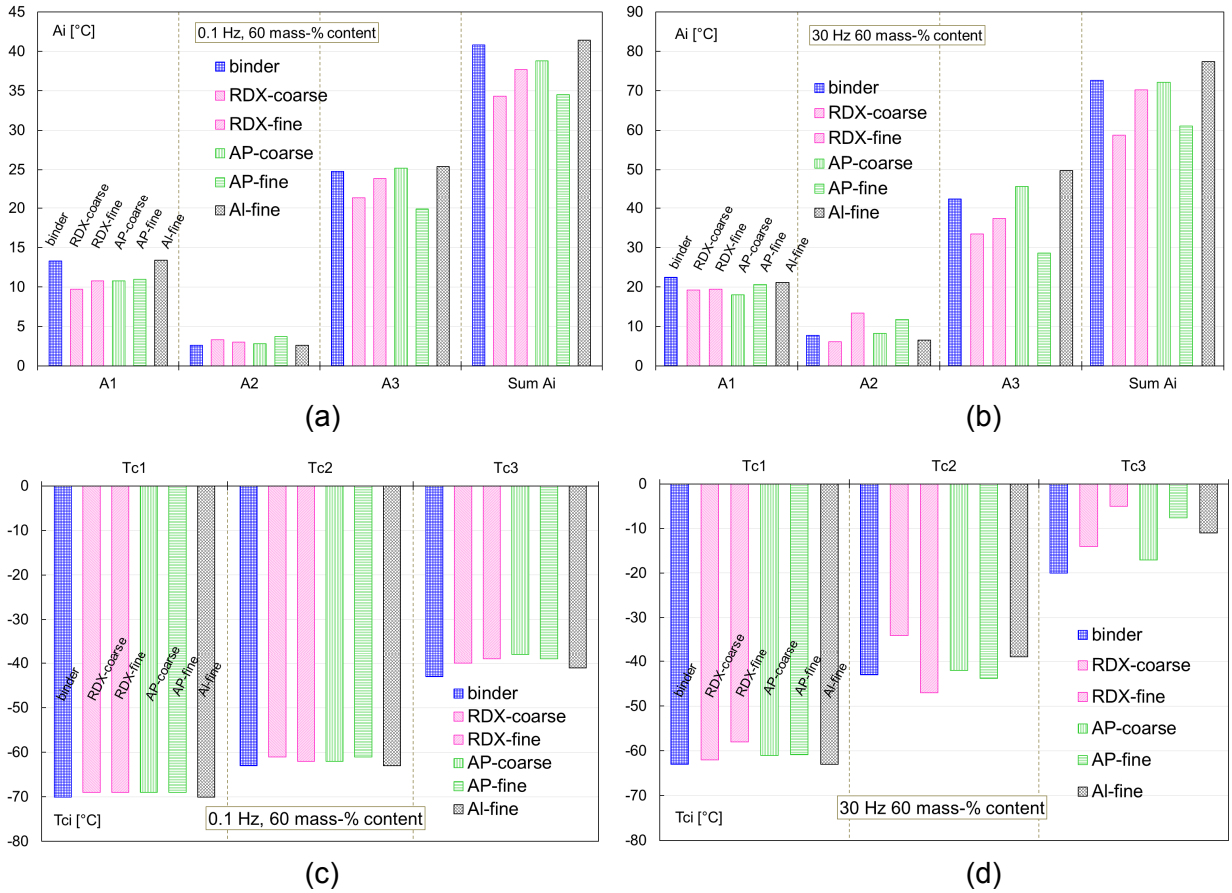

Figure 17: Comparison of the modelling parameters area Ai (a and b) and Gauss peak temperature Tci (c and d) at 0.1 Hz (left) and 30 Hz (right) deformation frequency, composites with 60 mass-% filler. In each figure one series of the columns is named, the naming is always equal for the other series.

Two parameters are important for composites and are discussed now in more detail. One parameter is the intensity or area parameter A_i. The other parameter is the peak temperature Tc_i. When the intensity of the glass-rubber transition expressed by A is small, the reasons can be: (1) more hindrance in mobility for the pre-polymer or (2) a more elastic behavior of the polymer, means a more dominant elastic (storage) shear modulus. The temperature of the glass-rubber transition approximated by Tci is decisive for the use or application. Composites with elastomeric binders have the operational in-service above the glass-rubber transition temperature, this means it must be low enough to afford low temperature use.

The following refers to Fig 17a till Fig. 17d. Regarding the sum of the peak areas ($\sum A_i$), filling the binder with AP coarse particles had nearly no effect on the area. Fine AP however causes an overall depreciation of A_i parameters. This means that the polymer gained more in the elastic shear modulus than in the loss shear modulus – one can say the sample is more elastic and less viscous compared to AP coarse. But the higher the tanδ or the area of it the greater the binder part which can perform the transition from glassy to rubbery transition. RDX has a reversed effect: the filling with coarse particle size decreases the sum of A_i parameters. SEM analysis of AP fine and RDX coarse particles (Fig. 18b and 18c) show that both are less round, means they have more irregular geometry and edges, whereas coarse AP and fine RDX (Fig. 18a and Fig.18d) have a shape closer to a sphere or are at least rounded. This is an indication that the sum of A_i parameters is more affected by the AP and RDX particle shape than by their size. The round particles exert less mobility restrictions but create a higher amount of amorphous binder structures instead of rigid ones. The rigid binder parts cannot transform from glassy to rubbery state. The both Al powders have more or less rounded particles (Fig.18e and 18f). See also Fig. 19 and Fig. 20.

Paper number 20069, Text pages 1 to 30, Session 3B, on 2018 NDIA-IMEMTS, event number 8550, April 23-29, 2018, Portland Oregon, USA. http://www.ndia.org/events/2018/4/23/imem

Area A_3 is the one of the loss factor peak attributed to the transition of binder parts with more mobility restriction, i.e hindrance of chain mobility by filler-particle interactions and by the cross-link ranges. But these types of hindrances are not rigidity promoting as this is caused by increasing cross-link density during ageing. It is evident from the results that the addition of Al particles has a stronger effect on increasing the value of parameter A_3 than the other particles have, and this effect is more pronounced when deformation frequency is increased.

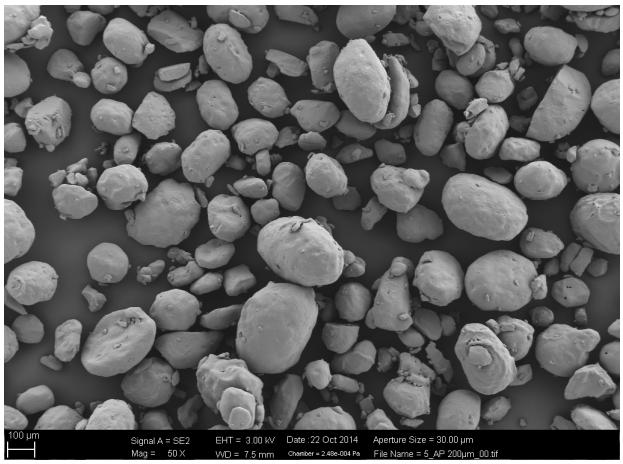

(a) coarse AP, rounded

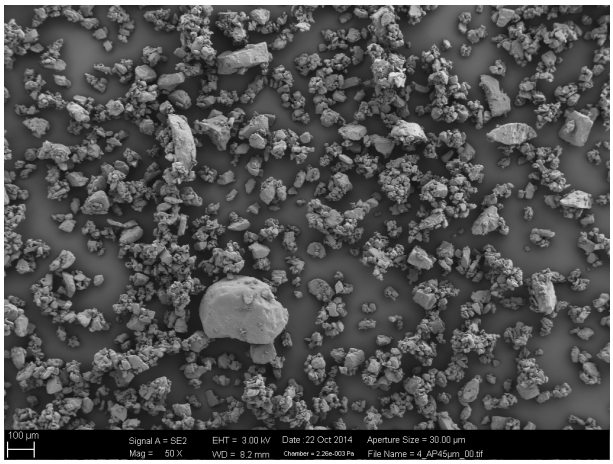

(b) fine AP, not rounded

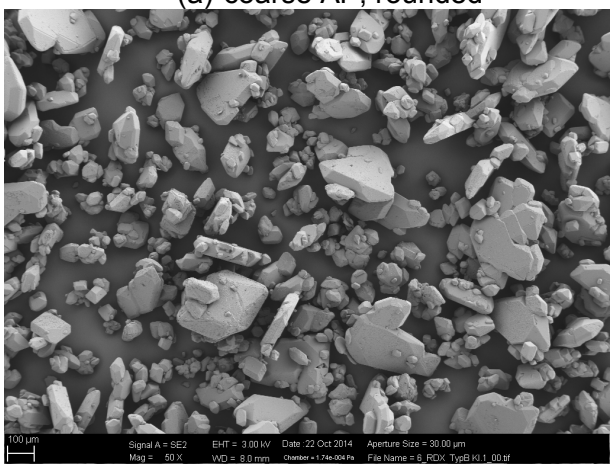

(c) coarse RDX, not rounded

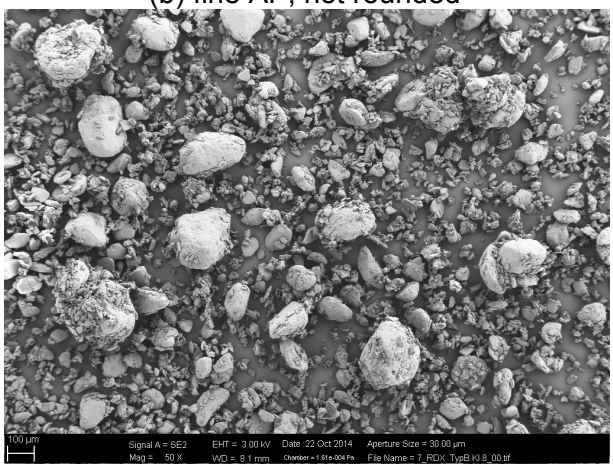

(d) fine RDX, rounded

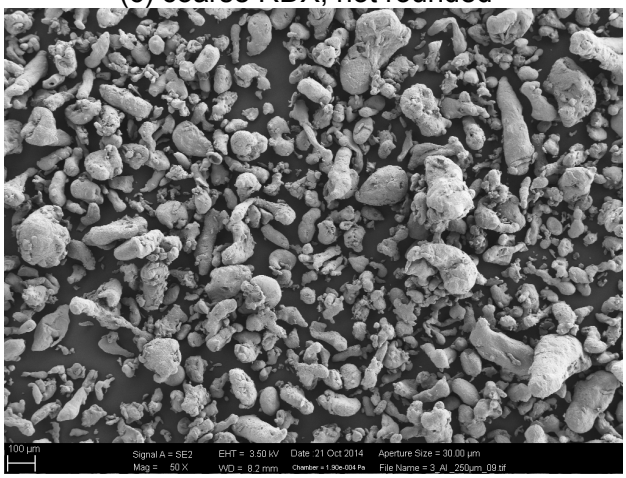

(e) coarse Al, rounded

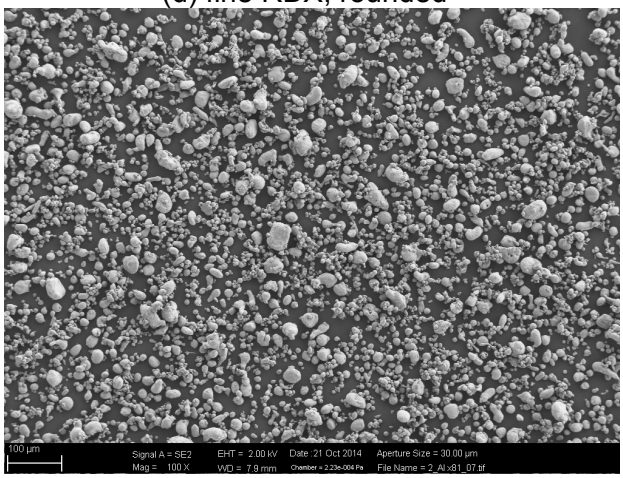

(f) fine Al, rounded

Figure 18: SEM images (maginification of 50X) of the particles used here; (a) coarse AP (b) fine AP; (c) coarse RDX; (d) fine RDX; (e) coarse Al; (f) fine Al. Scale of 100µm.

On the surface of aluminum particles species as Al hydroxide can be formed due to contact of the metallic Al with air (oxygen) and humidity. It was already discussed in the literature that the OH on Al may capture one end of isocyanate molecules [3], leaving less isocyanate groups to react with pre-polymer and more not bonded polyol chain ends are available. This may change the R_{eq} in the binder near the Al particles. According to literature, the second apparent loss factor peak in HTPB-based solid propellants, represented mainly by the EMG-3 (peak 3), can be caused by two effects:

(1) from the flow of free polymer chains in the polymer network with a reptation mechanism (snake like movement). If more polymer or polyol chains are available to move near the particle due to isocyanate "capture" near the aluminum surface, one could expect an increase in A_3 value [19];
(2) from a more intense intermolecular interaction between Al and HTPB than between the polyol and AP.
(2-1) From molecular dynamics one knows that metallic Al has higher intermolecular interaction energies with HTPB than AP. Therefore, the hindrance of HTPB chains is larger, which extends the range of the polymer shell around Al and this effect increases the intensity of the loss factor [20, 21]. Due to stronger interactions, the Al exert more hindrance on the mobility of the HTPB chains in the polymer shell around the particles [7,8,9]. As a consequence the glass-rubber transition temperature of such binder fractions is shifted to higher temperature values compared to not mobility restricted HTPB chains (see Tc_3 parameters).
(2-2) Secondly, because of the increased binder part in this fraction, it creates a relative intense glass-rubber transition in the polymer chains, since the mobility restriction imparted by Al is not high enough to hinder the transition to take place.
(2-3) Another effect is the stronger chemical bonding of Al particles to the network, when isocyanate attaches to the Al surface via its OH groups and bonds it to the binder via the second NCO group. This enlarges the polymer shell around Al particles and the intensity of A_3 is increased.

This effect of reducing mobility can be also the case, if one has increasing cross-linking between the polymer chains in the neighborhood of particles, which form then a more rigid amorphous region and the transition intensity is reduced, but the storage modulus increases. This was found with ageing of composite RP [7].

Regarding the Tci parameters, Tc_1 is nearly not affected, independent of particle size or type. Tc_2 and Tc_3 are increased (become less negative), and the increase is more pronounced at higher deformation frequencies, especially with fine particle sizes. This is an indication that an increase in solid filler tend to enhance chain mobility restrictions, affecting the T_g^{res}, and corroborating the results shown in Table 2 and in Figure 17.

In Fig. 19 and Fig. 20 some features are expressed and will be discussed. The base is the loss factor curve of the unfilled binder. The Al-coarse composite curve coincides nearly completely along the first peak with the curve of the unfilled binder. In the range of the second evident peak, the Al-coarse causes higher intensity than the binder, not much, but significantly. This is indicative for the build-up of a polymer shell around the Al particles. Another feature is shown by the RDX-coarse composite. From Fig. 18c is clear that RDX coarse has not rounded particles. Plates can be identified. Such particle shapes hinder effectively chain mobility and therefore the first loss factor peak is reduced more than with rounded particles. This is expressed also in the second evident peak with an intensity lower than the one of the unfilled binder. In Fig. 20 the situation is reverse with AP-fine and RDX-fine. Now AP-fine is not rounded but RDX-fine is. AP-fine reduces the intensity of first peak a bit more than RDX fine, but the second peak is now reduced by AP-fine whereas RDX-fine opens (reduces) the interactions between the HTPB chains and the intensity increases. Pronounced said: RDX fine acts as a plasticizer in this binder part.

Paper number 20069, Text pages 1 to 30, Session 3B, on 2018 NDIA-IMEMTS, event number 8550, April 23-29, 2018, Portland Oregon, USA. http://www.ndia.org/events/2018/4/23/imem

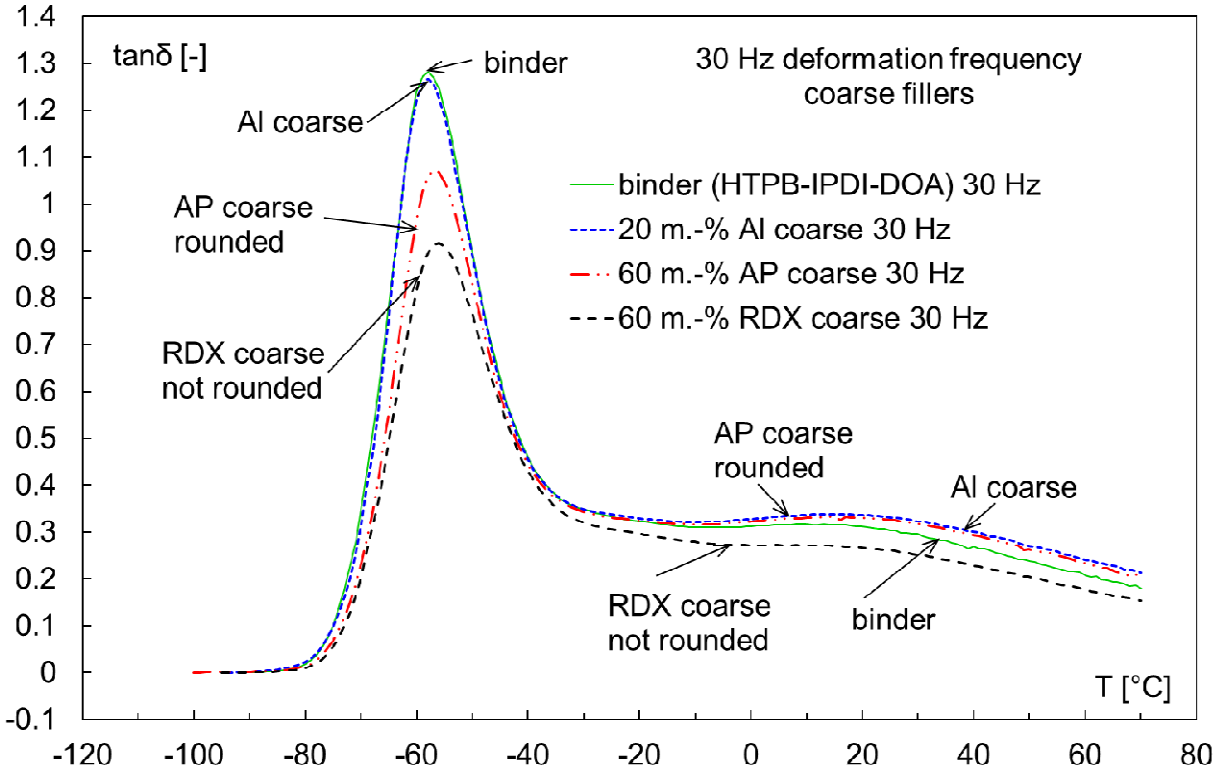

Figure 19: Four loss factor curves obtained at 30 Hz deformation frequency, comparison of three composites with **coarse** Al, AP and RDX with the unfilled binder.

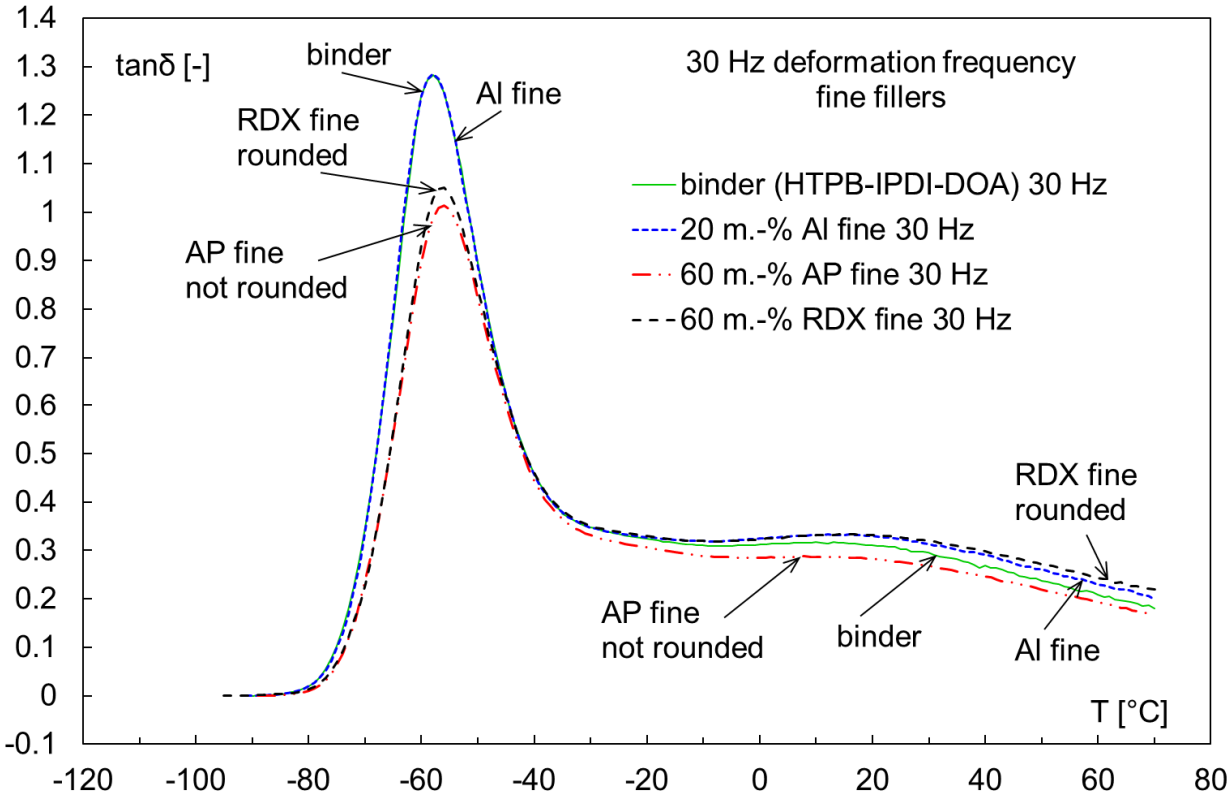

Figure 20: Four loss factor curves obtained at 30 Hz deformation frequency, comparison of three composites with **fine** Al, AP and RDX with the unfilled binder.

Paper number 20069, Text pages 1 to 30, Session 3B, on 2018 NDIA-IMEMTS, event number 8550, April 23-29, 2018, Portland Oregon, USA. http://www.ndia.org/events/2018/4/23/imem

3.4 Parameterization of loss factor shift with deformation frequency

The deformation frequency dependence of the thermo-mechanically activated glass-rubber transition can be expressed by Arrhenius parameterization. With the use of an Arrhenius type equation, Eq.(5), an apparent activation energy Ea_f of the binder chain separation process can be estimated. This is possible when the process under consideration is activatable by thermal energy and the change in free volume and molecular volume effects are not involved. Then the determined activation energy is representing molecular interaction energy.

$$f = f_0 \cdot \exp\left(-\frac{Ea_f}{R \cdot T_g(f)}\right) \qquad (5)$$

f applied deformation frequency [Hz];
f_0 pre-exponential factor [Hz], deformation frequency at T infintely high;
Ea_f activation energy for the shift of Tg (glass-rubber transition) by deformation rate hardening (strain rate hardening) of the material [kJ·mol^{-1}];
R general gas constant [8.31441 J·K^{-1} mol^{-1}];
T_g glass-rubber transition temperature [K] as function of deformation frequency, T_g is taken here in the maximum of the loss factor.

For the purpose of this parameterizations, it is necessary to determine the maximum temperatures T_g quite well. Therefore, the temperatures of the two evident maxima in the loss factor curve tanδ(T) = G''(T)/G'(T) of the samples were determined by using fits of polynomials of degree 3 just around the maxima and calculating the temperatures connected to the maxima. In Table 3 the data are compiled together with the Arrhenius parameters according to Eq.(5). Some fields of the Ea_f column are highlighted by boxes in Table 3. These data will be discussed in the following. First, a look on the Ea_f values of the pure binder. The first maximum at lower temperatures provides with 180.7 kJ/mol, which coincides well with data of HTPB-IPDI binder determined earlier with 196 kJ/mol [7,9]. The parameterization of the second maximum gives much smaller activation energies, for the binder it is 84.7 kJ/mol. This expresses the differences in interaction energies between the molecular regions of the binder. At lower temperatures the distances between the binder chain elements are smaller than at the temperature of the second maximum (-70°C to -58°C versus -28°C to +11°C) and therefore the energetic interaction is greater at lower temperatures.

From Table 3 the following can be concluded, see the highlighted parts in Ea_f column.

- AP coarse reduces Ea_f values in first peak with increasing content. AP coarse increases Ea_f values in second peak with increasing content. In second peak, AP coarse acts as intermolecular bond breaker, because the Ea_f value first decreases with small contents. The differences in peak temperature with regard to the pure binder are small in first peak. They increase with deformation frequency. In second peak, the differences to the reference are larger. AP fine causes a shift to lower temperatures in second peak
- RDX coarse reduces quite strongly Ea_f values in first peak with increasing content. In second peak no clear direction, more or less the Ea_f values stay constant. Also RDX fine reduces strongly the Ea_f value in first peak. The differences in peak temperature with regard to the pure binder are small in first peak. They increase with deformation frequency. In second peak the differences to the reference are larger.
- Al fine causes increase of Ea_f values in first peak with increasing content, same direction probably also in second peak. The interactions of Al via the polar surface groups (OH) may cause this. Al coarse shows also the effect of intermolecular bond breaking. The differences in peak temperature with regard to the pure binder are even

smaller in first peak compared to AP and RDX. They have the tendency to decrease with deformation frequency. But in second peak the differences to the reference are as large as with AP coarse and RDX coarse.

Table 3: Values of T_g^{unr} and T_g^{res} of the first and second peak of tanδ curve, given for all investigated samples, at deformation frequencies 0.1, 1.0, 10 and 30 Hz. The reference is the unfilled binder. The arrows in the column of activation energy show the change in values with changing filler content.

Sample	T_g^{unr} (first apparent peak)				Difference to reference				Ea_f [kJ.mol^{-1}]	ln(f_0 [Hz])
	0.1Hz	1.0Hz	10Hz	30Hz	0.1Hz	1.0Hz	10Hz	30Hz		
binder alone	-69.42	-65.58	-60.72	-57.95	*(reference)*				**180.7**	45.43
20% AP coarse	-68.86	-65.24	-60.28	-57.51	*0.56*	*0.34*	*0.44*	*0.44*	182.6	45.79
40% AP coarse	-68.78	-65.04	-60.11	-57.27	*0.64*	*0.54*	*0.61*	*0.68*	180.9	45.34
60% AP coarse	-68.63	-64.76	-59.62	-56.74	*0.79*	*0.82*	*1.10*	*1.21*	175.4	43.91
60% AP fine	-68.29	-64.38	-59.06	-56.16	*1.13*	*1.20*	*1.66*	*1.79*	172.3	43.04
20% RDX coarse	-68.95	-65.02	-60.09	-57.37	*0.47*	*0.56*	*0.63*	*0.58*	179.8	45.07
40% RDX coarse	-68.97	-65.01	-59.91	-57.22	*0.45*	*0.57*	*0.81*	*0.73*	176.7	44.30
60% RDX coarse	-69.58	-64.28	-59.02	-55.94	*-0.16*	*1.30*	*1.70*	*2.01*	154.9	38.78
60% RDX fine	-69.44	-64.56	-59.19	-56.19	*-0.02*	*1.02*	*1.53*	*1.76*	158.6	39.71
20% Al coarse	-68.90	-65.65	-60.76	-57.91	*0.52*	*-0.07*	*-0.04*	*0.04*	187.3	47.05
20% Al fine	-69.54	-65.71	-60.81	-57.95	*-0.12*	*-0.13*	*-0.09*	*0*	179.1	45.00
40% Al fine	-69.23	-65.69	-60.71	-57.77	*0.19*	*-0.11*	*0.01*	*0.18*	180.6	45.34
60% Al fine	-69.01	-65.56	-60.60	-57.80	*0.41*	*0.02*	*0.12*	*0.15*	184.0	46.18
	T_g^{res} (second apparent peak)				Difference to reference					
binder alone	-28.04	-13.65	2.52	10.87	*(reference)*				**84.7**	17.06
20% AP coarse	-29.42	-15.63	2.00	11.03	*-1.38*	*-1.98*	*-0.52*	*0.16*	80.7	16.33
40% AP coarse	-28.33	-14.14	2.94	12.46	*-0.29*	*-0.49*	*0.42*	*1.59*	81.3	16.37
60% AP coarse	-24.92	-11.96	4.22	14.98	*3.12*	*1.69*	*1.70*	*4.11*	85.4	17.03
60% AP fine	-29.25	-16.82	0.23	8.49	*-1.21*	*-3.17*	*-2.29*	*-2.38*	85.2	17.31
20% RDX coarse	-25.36	-12.23	4.57	14.24	*2.68*	*1.42*	*2.05*	*3.37*	85.1	17.00
40% RDX coarse	-24.34	-10.94	6.36	15.75	*3.70*	*2.71*	*3.84*	*4.88*	84.6	16.82
60% RDX coarse	-25.38	*Not well defined*			*2.66*	*Not well defined*				
60% RDX fine	-24.05	-11.76	4.96	15.47	*3.99*	*1.89*	*2.44*	*4.60*	86.1	17.14
20% Al coarse	-26.01	-11.7	6.13	15.09	*2.03*	*1.95*	*3.61*	*4.22*	81.7	16.29
20% Al fine	-25.88	-12.44	3.76	13.54	*2.16*	*1.21*	*1.24*	*2.67*	85.5	17.10
40% Al fine	-25.91	-11.74	4.35	11.32	*2.13*	*1.91*	*1.83*	*0.45*	88.7	17.74
60% Al fine	-23.25	-10.33	7.38	15.8	*4.79*	*3.32*	*4.86*	*4.93*	86.5	17.14

In short it is mentioned that some authors prefer the Williams-Landel-Ferry (WLF) equation for the temperature parameterization of quantities connected with polymers. Often it gives a better description than the standard Arrhenius equation, shown above. Especially to describe the so-

called horizontal shift factor obtained during construction of master curves is better described with WLF. But the WLF equation, Eq.(6), is completely congruent with the modified Arrhenius equation, Eq.(7), what was shown in a recent paper, see [23]. There also applications are shown and the difference in Ea_{0M} and Ea_f is discussed. An important outcome is that the second WLF invariant $C_1 \cdot C_2$ is proportional to activation energy Ea_{0M}, Eq.(8), and the first WLF invariant T_∞ is the same as T_{0M}, Eq.(9)

$$\lg\left(a_T(T,Tr)\ \ [-]\right) = \lg\left(\frac{f(Tr)}{f(T)}\right) = -\frac{C_1 \cdot (T - Tr)}{C_2 + (T - Tr)} \tag{6}$$

$$f = f_{0M} \cdot \exp\left(-\frac{Ea_{0M}}{R \cdot (T_g(f) - T_{0M})}\right) \tag{7}$$

f	applied deformation frequency [Hz];
f_{0M}	pre-exponential factor [Hz];
Ea_{0M}	activation energy for the shift of T_g by strain rate hardening [kJ·mol^{-1}];
R	general gas constant [8.31441 J·K^{-1} mol^{-1}];
T_g	glass-rubber transition temperature [K] as function of deformation frequency
T_{0M}	mobility freezing reference temperature, identical to T_∞ of WLF equation (spoken T zero mobility)

$$Ea_{0M} = R \cdot C_1 \cdot C_2 / \lg(e) \tag{8}$$

$$T_{0M} = Tr - C_2 = T_\infty \tag{9}$$

4. Summary and conclusions

The formulations with low to medium to high filler content could be manufactured successfully by using a turning machine during curing, in order to get a homogenous distribution of the filler particles all over the binder matrix volume. For the mixing, a planetary–rotary mixer was used to produce smaller amounts of composites. The binder is based on HTPB-IPDI polyurethane with 5 mass-% DOA added. The equivalent ratio R_{eq} (NCO / OH) = 0.85, as typical for CRP type formulations. Fillers have been AP coarse and fine (202 and 43 µm), RDX coarse and fine (233 and 61 µm) and Al coarse and fine (130 and 21 µm). No bonding agents have been used. Content steps were 20, 40 and 60 mass-% in binder.

The possible effects of filler concentration on the visco-elastic properties of the composites have been investigated with DMA (dynamic mechanical analysis) in torsion mode. Two properties of the loss factor curves have been used, determined at four deformation frequencies: The deformation rate caused shift of the temperatures at the two apparent maxima and the shape of the curves. The temperature shift was parameterized by a standard Arrhenius expression. The shape analysis was performed by applying three EMG distributions to each loss factor curve, providing with intensities for binder parts with different glass-rubber transition temperatures, caused by different molecular mobilities in the binder parts.

Main results are:
AP and RDX cause more changes in intensity of first peak of loss factor than Al fine particles. The temperature in first maximum is not much changed by the fillers at all concentrations. Al particles change least in comparison to unfilled binder. The changes in temperature of second peak are greater. The intensity changes in loss factor were determined via EMG modelling. AP fine decreases intensity compared to AP coarse. The effect is vice versa with RDX. It seems

that particle shape has a distinct influence. The rounder particles have a less hindrance effect on molecular mobility and finally increase the intensity in the transition glass to rubber. Increasing content of AP and RDX increase the elastic (storage) modulus G' and a bit increase in the loss modulus G'' also. But in total the main peak in loss factor curve is reduced in intensity. From the change in loss factor intensity and temperature shifts, it is concluded that Al particles have a stronger molecular interaction with the binder than AP and RDX, if no bonding agents are used.

5. Abbreviations

Al	aluminium, powder, fuel
AO	antioxidant
AP	ammonium perchlorate, powder, oxidizer
BLC	baseline correction of loss factor
BO	bonding agent
CRP	composite rocket propellant
CT	computer tomography
DMA	dynamic mechanical analysis
DOA	dioctyl adipate or better di-(ethyl-hexyl) adipate, plasticizer
EMG	exponentially modified Gauss distribution
HMX	Octogen, octahydro-1,3,5,7-tetranitro-1,3,5,7-tetrazin, high explosive compound
HTPB	hydroxyl terminated polybutadiene, binder pre-polymer
HX	abbreviation for high explosive formulation
IPDI	isophorone diisocyanate, cross-linker or curing agent
RDX	hexahydro-1,3,5-trinitro-1,3,5-triazin, high explosive compound (known also as cyclo-trimethylene-trinitramine, royal demolition explosive, research department explosive, Hexogen, Cyclonite, T4)
SEM	scanning electron microscopy
G'	Storage or elastic shear modulus
G''	Loss or viscous shear modulus
tanδ	Loss factor, tanδ = G''/G'

6. References

[1] Sara Cerri, Manfred A. Bohn, Klaus Menke, Luciano Galfetti.
Ageing Behavior of HTPB Based Rocket Propellant Formulations.
Central European Journal of Energetic Materials, 6(2), 149-165, **2009**.

[2] Manfred A. Bohn
Impacts on the loss factor curve and quantification of molecular rearrangement regions from it in elastomer bonded energetic formulations.
in 'Energetics Science & Technology in Central Europe' edited by R. Armstrong, J. Short, and D.K. Anand. CALCE EPSC Press, University of Maryland, College Park, MD 20742, USA. **2012**.

[3] Sara Cerri, Manfred A. Bohn.
Separation of molecular mobility ranges in loss factor curves by modeling with exponentially

modified gauss distributions.
Paper 87, pages 87-1 to 87-16 in Proceed. of 41th International Annual Conference of ICT on 'Energetic Materials – High Performance, Insensitive Munitions, Zero Pollution', June 29 to July 2, 2010, Karlsruhe, Germany. ISSN 0722-4087. Fraunhofer-Institut für Chemische Technologie (ICT), D-76318 Pfinztal-Berghausen. Germany. **2010.**

[4] Manfred A. Bohn, Sara Cerri.
Aging Behavior of ADN Solid Rocket Propellants and Their Glass-Rubber Transition Characteristics. pages 771 to 800 in
De Luca L.T., Shimada T., Sinditskii V.P., Calabro M. (eds) (2016) Chemical rocket propulsion: A comprehensive survey of energetic materials. ISBN 978-3-319-27746-2. DOI 10.1007/978-3-319-27748-6. Springer International Publishing AG, CH-6330 Cham, Switzerland. **2016.**

[5] Manfred A. Bohn and Sara Cerri.
Molecular mobility in binder systems.
Proc. 42nd International Annual Conference of ICT on 'Energetic Materials', June 28 to July 1, 2011, Karlsruhe, Germany. ISSN 0722-4087. Version CD-Proceedings. Paper 96, pages 96-1 to 96-33, **2011.**

[6] Manfred A. Bohn, Günter Mußbach, Sara Cerri.
Influences on the Loss Factor of Elastomer Binders and its Modeling.
Paper 60, pages 60-1 to 60-43 in Proceedings of the 43rd International Annual Conference of ICT on 'Energetic Materials – Synthesis, Characterisation, Processing', June 26 to 29, 2012, Karlsruhe, Germany. ISSN 0722-4087. Fraunhofer-Institut fuer Chemische Technologie (ICT), D-76318 Pfinztal. Germany. **2012**.

[7] Sara Cerri, Manfred A. Bohn, Klaus Menke, Luciano Galfetti,
Ageing of HTPB/AL/AP rocket propellant formulations investigated by DMA measurements.
Propellants, Explosives, Pyrotechnics, vol. 38, pp. 190-198. **2013**.

[8] Manfred A. Bohn, Günter Mußbach, Sara Cerri.
Modeling of loss factors of elastomer binders of high explosive charges and composite rocket propellants to separate binder fractions with different molecular mobility used to follow aging.
Proc. of 10th Int. Symposium on Special Topics in Chemical Propulsion & Energetic Materials, Poitiers, **2014.**

[9] Sara Cerri, Manfred A. Bohn, Klaus Menke, Luciano Galfetti,
Aging of ADN Rocket Propellant Formulations with Desmophen-Based Elastomer Binder.
Propellants, Explosives, Pyrotechnics, vol. 39, pp. 526-537. **2014**.

[10] Mauricio F. Lemos, Guenter Mussbach, Manfred A. Bohn.
Evaluation of filler effects on the dynamic mechanical analysis of elastomer applied as binder in composite propellants.
J. Aerospace Tech. Management. Paper in production.

[11] Manfred A. Bohn, Günter Mußbach, Gunnar Kronis
Data interpretation and comparison of DMA results from HTPB-IPDI bonded composite elastomer samples used in an international Round Robin Test.
Paper 131, pages 131-1 to 131-19. CD-Proc. of the 47th International Annual Conference of ICT on 'Energetic Materials – Synthesis, Characterization, Processing', June 28 to July 1, 2016, Karlsruhe, Germany. ISSN 0722-4087. Fraunhofer-Institut fuer Chemische Technologie (ICT), D-76318 Pfinztal, Germany. **2016.**

[12] Tijen Seyidoglu, Manfred A. Bohn.
Effect of Butacene® on ageing of composite propellants.
Proc. of the 19th NTREM (New Trends in Research of Energetic Materials), Pardubice, pages 904-925. Pardubice, Czech Republic, April 20-22, **2016**.

[13] Tijen Seyidoglu, Manfred A. Bohn, Guenter Mussbach.
Accelerated Aging and Cure Kinetics of Butacene® Containing Composite Propellants
Paper 78, pp 78-1 to 78-22, on CD Proceedings of the 47th International Annual Conference of ICT on 'Energetic Materials – Synthesis, Characterization, Processing', June 28 to July 1, 2016, Karlsruhe, Germany. ISSN 0722-4087. Fraunhofer-Institut fuer Chemische Technologie (ICT), D-76318 Pfinztal. Germany. **2016**.

[14] Tijen Seyidoglu, Manfred A. Bohn.
Characterization of Aging Behavior of Butacene® Based Composite Propellants by Loss Factor Curves.
Propellants, Explosives, Pyrotechnics, in production, **2017.**

[15] Tijen Seyidoglu, Manfred A. Bohn.
Modelling of Loss Factor Curves Obtained by Torsion-DMA of HTPB and GAP Based Binders manufactured with Different Curing Agents and Plasticizers.
Proc. 46th International Annual Conference of ICT, June 23 to 26, 2015, Karlsruhe, Germany. ISSN 0722-4087. Paper 118, pp 118-1 to 118-26, **2015.**

[16] Mauricio F. Lemos, Manfred A. Bohn.
The effect of plasticizers on the glass-to-rubber behavior of Desmophen® 2200 based elastomers used for composite propellants.
Paper 22, pages 22-1 to 22-26 in Proc. of the 46th International Annual Conference of ICT on 'Energetic Materials – Performance, Safety and System Applications', June 23 to 26, 2015, Karlsruhe, Germany. ISSN 0722-4087. Fraunhofer-Institut fuer Chemische Technologie (ICT), D-76318 Pfinztal. Germany. **2015.**

[17] Mauricio F. Lemos, Manfred A. Bohn.
Evaluation of the effect of plasticizers on the DMA loss factor, the thermal and mechanical properties of Desmophen® 2200- based elastomers used for composite propellants.
Proc. of the 18th NTREM (New Trends in Research of Energetic Materials), Pardubice, p. 670-694, **2015.**

[18] Mauricio F. Lemos, Manfred A. Bohn.
DMA of polyester-based polyurethane elastomers for composite rocket propellants containing different energetic plasticizers.
J. Therm. Anal. Calorim., DOI 10.1007/s10973-016-5945-1, 2016, **2017.**

[19] A. Azoug, R. Nevière, A. Constantinescu,
Molecular Origin of the influence of the temperature on the loss factor of solid propellant. Propellants, Explosives, Pyrotechnics, 40, pp.469-478, **2015.**

[20] Michael M. Nardai, Manfred A. Bohn.
Cohesion properties in PBX and composite propellants – computational results and experimental aspects.
Paper 19, pages 19-1 to 19-17 in Proc. of the 46th International Annual Conference of ICT on 'Energetic Materials – Performance, Safety and System Applications', June 23 to 26, 2015, Karlsruhe, Germany. ISSN 0722-4087. Fraunhofer-Institut fuer Chemische Technologie (ICT), D-76318Pfinztal. Germany**. 2015**.

[21] Michael M. Nardai, Manfred A. Bohn.
Wetting of oxidizer particles by binder and plasticizer molecules – microcalorimetry experiments and computer simulations.
Proc. of the 18th NTREM (New Trends in Research of Energetic Materials), Pardubice, pages 212-228. Pardubice, Czech Republic, April 15–17, **2015**.

[22] H.L. Ornaghi, Jr.,A.S. Bolner, R. Fiorio, A.J. Zattera, S.C. Amico.
Mechanical and dynamic mechanical analysis of hybrid composites molded by resin transfer molding.
Journal of Applied Polymer Science, 118, pp. 887–896, **2010**.

[23] Manfred A. Bohn,
The connection between WLF equation and Arrhenius equation.
Proceed 21th International Seminar NTREM (New Trends in Research of Energetic Materials), April 18-20, **2018**. Pages 64 to 81. University of Pardubice, Pardubice, Czech Republic. Editors: Jiří Pachman, Jakub Šelešovský. Conference and proceedings number: 21. Published by University of Pardubice, Czech Republic, April **2018**. Pages 1227 + 16. ISBN 978-80-7560-136-0 (Print), ISBN 978-80-7560-137-7 (CD).